

The Effective Notch Stress Approach for a Tubular Joint

by

O.L.A.B. (Olmo) Middeldorp



The Effective Notch Stress Approach for a Tubular Joint

by

Olmo Luigi Antoon Briglia Middeldorp

to obtain the degree of Master of Science

at the Delft University of Technology,

to be defended publicly on Friday 2 June 2023, at 14:30

Student Number 4444949
Study MSc Civil Engineering
Track Structural Engineering
Specialisation Structural Mechanics
Project period 1 September 2022 - 2 June 2023

Committee	Prof.dr.ir. L.J. (Bert) Sluijs	Delft University of Technology
	Dr.ir. F.P. (Frans) van der Meer	Delft University of Technology
	Prof.dr. M. (Milan) Veljkovic	Delft University of Technology
	Dr.ir. A. (Alexander) Verbart	Ramboll Group A/S



Preface and Acknowledgements

This MSc thesis report marks the culmination of my studies at TU Delft, a journey filled with memorable experiences. It all began in 2015 when I pursued my childhood dream of becoming a renowned architect by starting a BSc in Architecture. However, I soon discovered that my true passion lay in tackling the complex mechanical aspects of large and unconventional structures. This realisation led me to enrol in the BSc program in Civil Engineering the following year and made me continue with the MSc in Structural Engineering in 2020. Besides my studies, I had the opportunity to work on a project related to offshore wind turbines, where I was fortunate enough to witness the installation of a turbine firsthand. This experience ignited a fascination within me. The large scale of these structures and the unique challenges associated with supporting wind turbines at sea drive my interest.

Therefore, I am grateful to conduct this thesis in collaboration with Ramboll, a leading company in offshore wind engineering, and it was a pleasure to combine my passions for structural mechanics and offshore engineering in this research. Reflecting on the past nine months of my thesis work, I would like to extend my thanks to the following individuals.

Bert Sluijs and Frans van der Meer, for their genuine interest in my work and constructive feedback. Their positive communication played a significant role in motivating me. I would also like to extend my appreciation to Milan Vejlovic, who joined the committee at a later stage, for showing the same level of interest and support.

Alexander Verbart, for his frequent guidance, insightful comments and sincere interest. I appreciate his support in providing me with the freedom to explore and investigate the topics I was passionate about, without pushing me in any direction. Additionally, I am grateful to Alex for being a great sounding board on both a technical and personal level. His mentorship has undoubtedly contributed to the quality of this research and my attitude towards the project.

Ronnie Pedersen, for giving me the opportunity to collaborate with Ramboll on this thesis and for supporting my move to Copenhagen. Ronnie's assistance and provision of everything needed, have contributed to the smooth execution of this project.

Martin Jepsen, Kim Kamau and Mikkel Larsen, for their teaching, guidance, reviews and collaboration on my project. Our frequent talks have consistently helped me to move forward.

Reza Azizi, Thomas Holm-Jensen, Marc Foßberg, Karsten Schürmann, Afrim Berisha, Vishal Vishwakarma, Joachim Christiansen, Stephen Phillips, Marcos Gómez, Jacob Fisker and Paul Misic, for their interest and guidance, and for making me feel at home at the office.

Olmo Middeldorp, May 2023

"The noblest pleasure is the joy of understanding" ~ Leonardo da Vinci

Abstract

Offshore wind energy production is increasing rapidly and optimising the design of support structures has the potential to significantly reduce steel and costs. Jacket structures are commonly selected for deeper waters, and the design of these structures is primarily influenced by the fatigue performance of the tubular joints. The fatigue resistance of these joints can typically be evaluated using different stress assessment methods, each associated with a corresponding S-N curve. While the Hot Spot Stress (HSS) approach is commonly used for design purposes, the Effective Notch Stress (ENS) approach offers higher accuracy by taking into account the stress concentration originating from the weld profile. Consequently, the ENS approach has the potential to provide less conservative fatigue life estimations, leading to the reduction of steel and costs. However, the application to and research of the ENS approach for tubular joints is limited. Therefore, the objective of this thesis is to investigate the application of the ENS approach on a tubular joint. The research was divided into three parts, including an investigation on the required FE mesh, a study on sub-modeling of the ENS approach and a comparative analysis on the fatigue life predictions between the HSS and ENS approaches.

The FE mesh required for the ENS approach was evaluated on a cruciform joint according to the DNV-RP-C203 [1] validation methodology and the Stress Concentration Factors (SCFs) values obtained for different mesh configurations were compared. Two mesh variants were developed, and different element sizes in the notch were evaluated. The results show that with a maximum element size in the notch equal to 0.39 mm, according to DNV [1], unacceptable SCF errors are obtained of -4% and 4%. Furthermore, with a maximum notch element size of 0.25 mm, according to IIW [2], SCF errors of -0.3% and -2.2% were obtained, indicating that accurate results can be obtained but are not guaranteed. Additionally, the accuracy of the mesh was found to be primarily influenced by the number of nodes surrounding the notch, rather than the size of the elements in the notch.

The accuracy of sub-modeling for the ENS approach on a tubular T-joint was evaluated by varying global modeling choices and sub-model sizes. The accuracy was measured by comparing sub-modeling stress results against those from a global T-joint FE model with the ENS approach applied. The results show that a global model composed of 3D elements with a weld profile that corresponds to the sub-model is recommended. Simplifying the global model by excluding the weld profile or using 2D elements has been found to provide inconsistent and inaccurate results. Moreover, a sub-model of the weld area with a size as small as 1.67° of the brace radial angle has been found to provide consistent results. Thereby, sub-modeling reduces the required mesh size by a factor of 15, compared to the global modeling approach. Additionally, a rather surprising maximum principal stress error of approximately -6% was observed as a result of sub-modeling for all varied load types and sub-model sizes.

A comparative study between the HSS and the ENS approach was conducted for the computed fatigues of a tubular T-joint. Various FE models were composed for the T-joint subjected to different load cases, and equivalent SCFs were computed by introducing a Correction Factor (CF) based on the S-N curves of both approaches. The results show that the ENS approach provides a lower computed fatigue life over the HSS approach when applied to a tubular joint. This discrepancy is attributed to the FAT225 S-N curve, used for the ENS approach, which is not tailored for tubular joints but for welded straight plates. For the HSS approach, the choice of element type (2D vs 3D) and the inclusion of a weld profile have a significant effect on the stress distribution and the resulting fatigue life prediction. It was found that a model consisting of 3D elements with the inclusion of a weld profile yields the longest computed fatigue life for a tubular joint.

To conclude, the application of the ENS approach was investigated for a tubular joint, by evaluating the mesh sensitivity, examining the accuracy of sub-modeling and comparing the computed fatigue lives with those from the HSS approach. Further research is recommended to improve the computational efficiency of the ENS mesh and to achieve a deeper understanding of the -6% error found by sub-modeling. Additionally, the development of an S-N curve tailored for tubular joints is suggested to improve the accuracy of the ENS approach for this type of joint.

Contents

Preface and Acknowledgements	i
Abstract	ii
Nomenclature	v
Notations	v
Abbreviations	v
1 Introduction	1
1.1 Offshore Wind Turbine Support Structures	1
1.2 Jacket Structure	1
1.3 Fatigue Life of Welded Components	2
1.4 Computational Modeling of Jacket	4
1.5 Stress Concentrations in Tubular Joints	5
1.5.1 Nominal Stress	6
1.5.2 Hot Spot Stress (HSS)	6
1.5.3 Effective Notch Stress (ENS)	7
1.6 Thesis Objectives and Outline	9
2 FE Mesh for the ENS Approach	11
2.1 Research Objectives	11
2.2 Methodology	11
2.3 Results and Discussion	13
2.4 Conclusions	16
3 Sub-Modeling for the ENS Approach	17
3.1 Research Objectives	17
3.2 Methodology	17
3.2.1 Global Model Parameters	18
3.2.2 Sub-Model Parameters	20
3.3 Results and Discussion	21
3.4 Conclusions	25
4 Fatigue Life Comparison of the HSS and the ENS Approach	27
4.1 Research Objectives	27
4.2 Methodology	27
4.2.1 T-Joint Experiment and Properties	28
4.2.2 FE Models	29
4.2.3 The S-N Curves	30
4.2.4 Comparison With the Fatigue Experiment	31
4.2.5 Comparison of the Equivalent SCFs	32
4.3 Results and Discussions	33
4.3.1 Comparison With the Fatigue Experiment	33
4.3.2 Comparison of the Equivalent SCFs	35
4.4 Conclusions	36
5 Conclusions and Further Research	37
5.1 Conclusions	37
5.2 Further Research	37

Bibliography	39
A HSS Extrapolation Points	40
B Variation of the Effective Notch Radius	41
C Displacements Around the T-joint Weld	42
D Supplementary Sub-Modeling Study	43
E Supplementary Results	45
E.1 Sub-Modeling Study	45
E.2 Comparison With the Fatigue Experiment	48
F Results T-Joint Experiment (Confidential)	49

Nomenclature

Notations

δ	relative error
$\Delta\sigma$	stress range
ν	Poisson's ratio
ρ^*	microstructural length
σ_a	stress amplitude
σ_{eff}	effective stress
σ_{max}	maximum stress
σ_{mean}	mean stress
σ_{min}	minimum stress
σ_{nom}	nominal stress
τ_{nom}	nominal shear stress
θ	angle between brace and chord
a	intercept of the S-N curve with the N axis
A	area
D	chord outer diameter
d	brace outer diameter
E	Young's modulus
F	force
f_y	yield strength
I	moment of inertia
J	polar moment of inertia
k	thickness exponent
K_t	stress concentration factor
m	negative inverse slope of the S-N curve
M	bending moment
N	number of load cycles
P_s	probability of survival
R	stress ratio
r	radius
r_{real}	real notch radius
r_{ref}	effective notch radius
s	multiaxiality coefficient
T	chord thickness
t	brace thickness
t_{ref}	reference thickness

Abbreviations

1D	One-Dimensional
2D	Two-Dimensional
3D	Three-Dimensional
AL	Axial Loading
CF	Correction Factor
DNV	Det Norske Veritas
ENS	Effective Notch Stress
FE	Finite Element
GPa	gigapascal
HSS	Hot Spot Stress
IIW	International Institute of Welding
IPB	In-Plane Bending
kN	kilonewton
kNm	kilonewton meter
mm	millimeter
MPa	megapascal
MW	Megawatt
OPB	Out-of-Plane Bending
SCF	Stress Concentration Factor
TM	Torsion Moment

1 Introduction

This chapter provides a brief introduction to support structures for offshore wind turbines, with a specific emphasis on the jacket structure. Furthermore, the challenges involved in the fatigue life design of these jacket structures are discussed, which form the basis for the thesis's objectives.

1.1 Offshore Wind Turbine Support Structures

Since the realisation of the first offshore wind farm in 1991 off the coast of Vindeby, Denmark, offshore wind energy production has been increasing rapidly. The industry has evolved from shallow waters with relatively small wind turbines to greater depths and larger turbines. The largest announced offshore wind turbines are currently reaching 15 MW, compared to the 5 MW wind farm by Vindeby which consisted of 11 turbines [3][4]. The capital cost for offshore wind projects completed in 2018 averaged \$4,353,000 per MW, with support structure costs estimated to comprise 20-25% of this total [5]. Therefore, optimization of the support structure design has the potential to substantially decrease costs.

To resist wave, current and wind loading, various offshore wind support structure types have been developed. An overview of the most common ones is depicted in Figure 1.1. Currently, most offshore wind turbines are founded on monopiles [6]. However, particularly influenced by water depth and seabed composition, different foundation solutions are used in the industry. In deeper waters, monopiles become large and uneconomical due to difficulty in fabrication and installation. In addition, structural design requirements like natural frequency and lateral resistance become a greater challenge. Therefore, in water depths of 30 to 60 meters, jacket structures provide a good alternative [7].

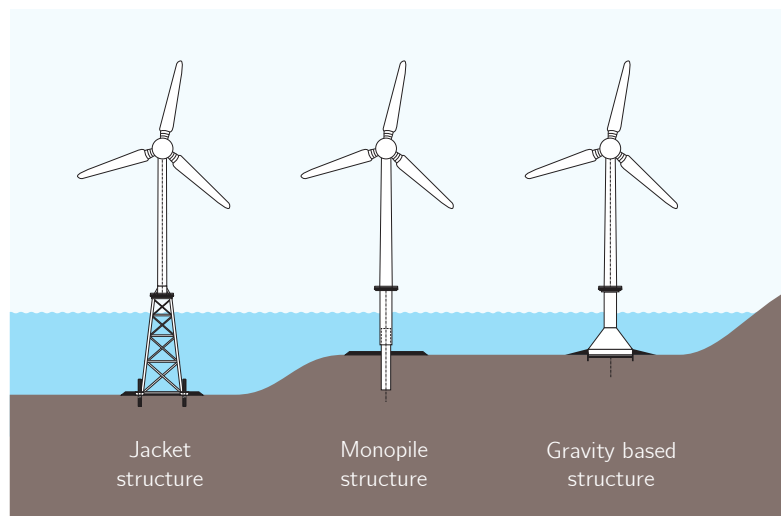


Figure 1.1: Common offshore wind support structure types [1].

1.2 Jacket Structure

A jacket structure is a welded tubular space frame consisting of battered legs supported by a lateral bracing system. The frame typically consists of three or four legs, known as chords, and the tubular beams between them, known as braces. The frame is typically constructed using steel, with chords and braces welded together. There are various types of beam connections present in a jacket, including K-, X-, Y- and T-joints. Figure 1.2 depicts an example of a jacket structure and Figure 1.3 features a schematic version of the structure with each component type labelled.

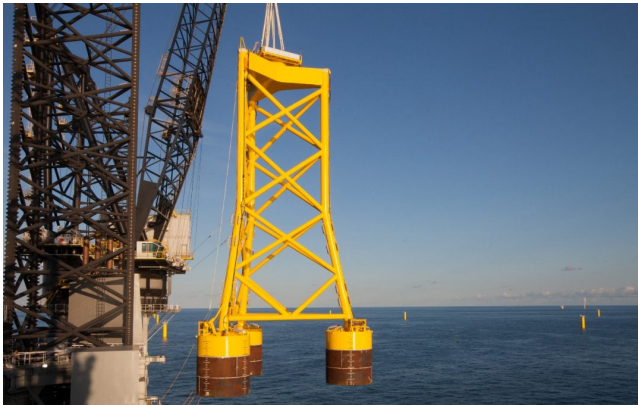


Figure 1.2: Example of a jacket structure [8].

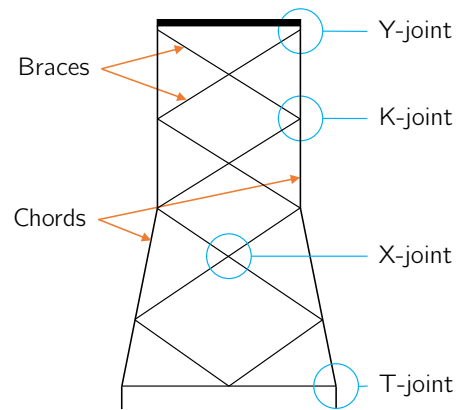


Figure 1.3: Beam and joint types.

Jacket structures are designed to withstand environmental loading with relatively low steel consumption. However, the welded connections between chords and braces are prone to fatigue damage. As a result, the fatigue life of tubular joints is the key factor governing the design life of jackets [9]. This is discussed in more detail in the following section.

The dimensions of tubular joints are commonly represented by the brace outer diameter (d), the brace thickness (t), the chord outer diameter (D), the chord thickness (T), and the angle between brace and chord (θ). Furthermore, the critical locations for failure in tubular joints can be identified by the crown and saddle points, which are four points along the weld, as illustrated in Figure 1.4. The cross-section of a weld is shown in Figure 1.5, where the leg thickness and throat thickness are specified, as well as the toes and the root, which are identified as critical points for failure.

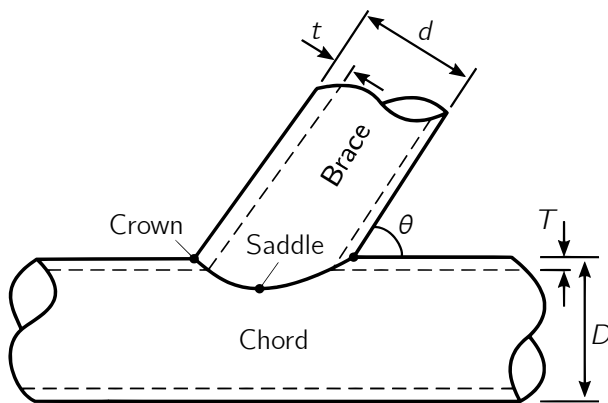


Figure 1.4: Tubular joint parameters.

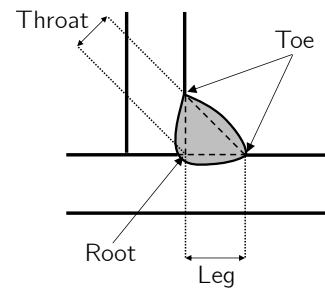


Figure 1.5: Weld parameters.

1.3 Fatigue Life of Welded Components

The fatigue phenomenon is described as structural failure without the material reaching its yield limit. Repeated loading within the elastic regime can cause crack initiation of material at microscopic level. Continued repeated loading can subsequently propagate the crack until structural failure. The total fatigue life can thus be distinguished by two phases, the crack initiation phase and the crack propagation phase.

No generally accepted quantitative measure exists that describes when the initiation phase is over and when the propagation phase starts. However, a visible or measurable crack length of 0.1 to 1.0 mm is often used

in practice to distinguish both phases. For welded components, the crack propagation phase covers most of the fatigue life, due to the presence of crack-like defects by the production [10].

Fatigue damage is governed by the difference in stresses in a certain time frame, rather than the maximum stress. This difference is typically referred to as the stress range, denoted as $\Delta\sigma$, or as the stress amplitude, denoted as σ_a . The relationship between these two terms is given by

$$\sigma_a = \frac{\sigma_{\max} - \sigma_{\min}}{2} = \frac{\Delta\sigma}{2}, \quad (1.1)$$

in which σ_{\max} and σ_{\min} respectively represent the maximum and minimum stress found in a defined time frame. In practice, a relationship between the mean stress and the stress amplitude is often observed, where an increase in amplitude also leads to an increase in mean stress. This relationship is expressed through a constant stress ratio (R), which is calculated as

$$R = \frac{\sigma_{\min}}{\sigma_{\max}}. \quad (1.2)$$

This results in a negative mean stress for $R < -1$ and a positive mean stress for $R > -1$. Experimental studies have shown that fatigue strength is negatively correlated with the mean stress, implying that higher tensile stresses result in lower fatigue life. Welded components are often subjected to residual stresses due to the manufacturing process, which are internal stresses that remain in the material even without the presence of external loading. Estimating or measuring residual stresses is challenging, and therefore, in practice, they are often taken into account by assigning a constant stress ratio of $R = 0.5$ [11].

In design calculations, S-N curves are commonly used to account for fatigue failure. The S-N curve describes the relationship between the stress range ($\Delta\sigma$) and the number of load cycles (N), for fatigue failure to occur. Typically, the S-N curve is derived from experimental data by using the stress range as the independent variable and fitting a curve to minimize the squared distance between the data points and the fitted curve. The resulting S-N curve then corresponds to a probability of survival of $P_s = 50\%$, known as the mean S-N curve. For design purposes, a higher probability of survival of $P_s = 97.7\%$ is generally used, which is based on the mean minus two standard deviations and is referred to as the design S-N curve. The S-N curve is typically plotted on a double logarithmic axis and divided into two linear regions separated by the knee-point, as shown in Figure 1.6. The first linear region, known as the low cycle fatigue range, is characterized by a negative slope typically equal to $m_1 = 3$. The second linear region, called the high cycle fatigue range, has a slope typically equal to $m_2 = 5$ or $m_2 = 0$, of which the latter indicates that no fatigue failure is expected to occur below a certain stress range.

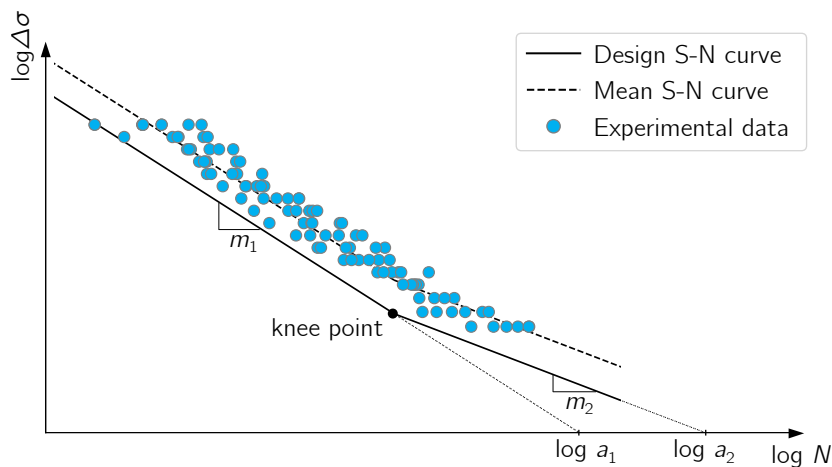


Figure 1.6: Characteristics of the S-N curve.

The relationship between the stress range ($\Delta\sigma$) and the number of load cycles (N) is expressed as

$$N \cdot \Delta\sigma^m = a, \tag{1.3}$$

with the intercept of the S-N curve with the N axis, denoted as a . However, this equation is typically adjusted to match the logarithmic axes of the curves, resulting in

$$\log N = \log a - m \log \Delta\sigma. \tag{1.4}$$

Additionally, the S-N curve may include a thickness effect which is incorporated using the reference thickness (t_{ref}) and the thickness exponent (k) as

$$\log N = \log a - m \log \left(\Delta\sigma \left(\frac{t}{t_{ref}} \right)^k \right). \tag{1.5}$$

The reference thickness is typically the thickness of the specimen for which the most tests were conducted, and the thickness exponent is derived from tests with various thicknesses.


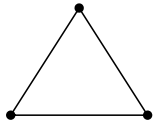
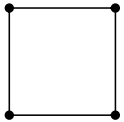
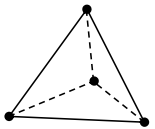
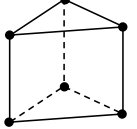
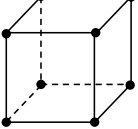
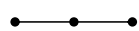
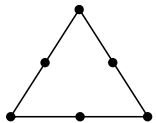
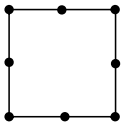
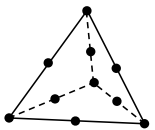
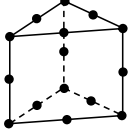
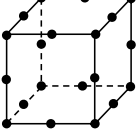
The selection of the appropriate S-N curve depends on several factors such as the material, the geometry, and the stress assessment method. For steel welded joints, mainly three methods for stress assessment exist with corresponding S-N curves: the nominal stress approach, the HSS approach and the ENS approach, which are further discussed in section 1.5.

1.4 Computational Modeling of Jacket

To design a jacket structure, it is necessary to perform structural calculations on a computational model that represents the jacket structure. Simulations of numerous load combinations must be carried out for design validation, and for each design iteration, the simulations must be repeated, resulting in a significant number of total simulations. Consequently, a computationally efficient model is crucial for the design process.

Generally, the FE method is used for such a model, in which the geometry of the structure is represented by a finite number of elements. All elements together form the so-called mesh of the FE model, which represents a discretization of the considered geometry. By introducing boundary conditions such as loads, displacements and/or constraints, a system of differential equations can be formed which are solved numerically. The elements of the FE model consist of nodes and different types can be distinguished in terms of dimension, geometry and polynomial order, as shown in Table 1.1.

Table 1.1: Element types.

	1D	2D		3D		
	Beam	Triangle	Quadrilateral	Tetrahedron	Prism	Hexahedron
Linear						
Quadratic						

While the use of 1D elements is the most computationally efficient method for modeling jackets, it lacks accuracy in local stiffness of the joints and the ability to estimate stress concentrations in the joints. To accurately represent the joint geometry in the structural calculations for a jacket, two approaches can be distinguished: parametric equations and FE modeling with 2D or 3D elements.

Modeling the complete jacket structure in 2D or 3D elements is computationally demanding. To overcome this problem, a sub-modeling approach in which only the joints are modeled with more detail can provide a solution. Sub-modeling, also known as multi-scale modeling, refers to the process of creating a sub-model of a larger global model and refining the geometry and/or mesh of the sub-model to obtain more accurate results in that region. The boundaries of the sub-model can be loads and/or displacements, which are coupled to the global model. It is important to note that these boundaries should be chosen carefully to avoid large errors, typically by selecting a location where stress gradients are lower. For a jacket structure, sub-modeling is commonly applied by using 1D elements for the global model, as shown in Figure 1.7, and 2D or 3D elements for the sub-models to represent the joints, as shown in Figure 1.8.

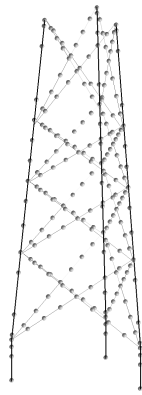


Figure 1.7: FE model of jacket with 1D elements.

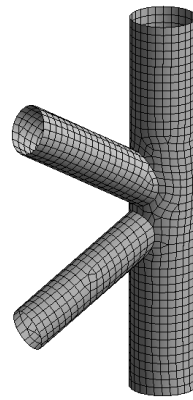


Figure 1.8: FE model of K-joint with 2D elements.

1.5 Stress Concentrations in Tubular Joints

Stress concentrations in tubular joints occur at the welds due to the geometry of the intersecting tubular elements and the profile of the weld. To account for stress predictions in tubular joints, SCF formulas were developed by M. Efthymiou in 1988 [12]. The SCF, also denoted as K_t , relates the nominal stress (σ_{nom}) in the tubular elements to the maximum stress (σ_{max}) in the following way:

$$SCF = K_t = \frac{\sigma_{max}}{\sigma_{nom}}. \quad (1.6)$$

Although the Efthymiou formulas provide a convenient way to obtain the SCFs, the formulas are not valid for all possible tubular joint geometries [1]. Additionally, the formulas are typically conservative compared to experimental values, with a coefficient of variance indicated to be 19% by ISO 19902 [13] and 20% by DNV-RP-C210 [14]. When the joint geometry is modeled in FE, more accurate SCF's can be obtained [15].

In FE analysis, stress singularity occurs at re-entrant corners, which are defined as inside corners with angles less than 180° . Stress singularity is defined as a point where the stress does not converge but keeps increasing towards infinity while the mesh size decreases, which results in an unrealistic stress value. As welds in tubular joints are located at re-entrant corners, weld stress assessment is a challenging task. The fatigue strength of welds can be calculated by different ways of stress assessment in combination with

an S-N curve. The most common approaches are the nominal stress approach, the HSS approach and the ENS approach, which are further discussed in subsection 1.5.1, subsection 1.5.2 and subsection 1.5.3, respectively.

1.5.1 Nominal Stress

In beam theory, the nominal stress is defined as the cross-sectional normal stress, without taking into account the effect of geometric discontinuities such as welds or intersecting beams, i.e. without considering stress concentrations. The nominal stress (σ_{nom}) due to an axial force (F) and a bending moment (M) is calculated as

$$\sigma_{nom} = \frac{F}{A} + \frac{My}{I}, \tag{1.7}$$

with the cross-sectional area (A), the moment of inertia (I) and the distance from the centroidal axis to the stress point (y). A graphical representation is depicted in Figure 1.9.

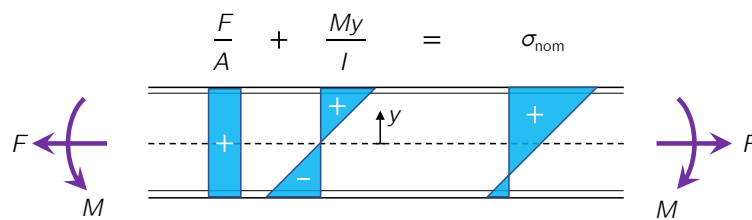


Figure 1.9: Graphical representation of the nominal stress.

To calculate the fatigue strength of a detail using the nominal stress approach, S-N curves specific to the geometry of the detail must be used. For tubular joints, the Efthymiou formulas are most commonly used to comply with S-N curves.

1.5.2 Hot Spot Stress (HSS)

The Hot Spot Stress (HSS) approach, also referred to as the structural stress approach, approximates the stress at the weld toe by extrapolating stress values a small distance away from the weld, as shown in Figure 1.10. The HSS comprises the nominal stress and the effect of the structural detail (the intersecting beams in a tubular joint) but not the local weld effect caused by the weld profile. Therefore, the extrapolation results in a lower stress than the actual stress present in the weld [15]. In fatigue calculations, this underestimation is compensated for by the S-N curves. For tubular joints, typically one S-N curve is used, also referred to as the T curve, which is further elaborated on in subsection 4.2.3.

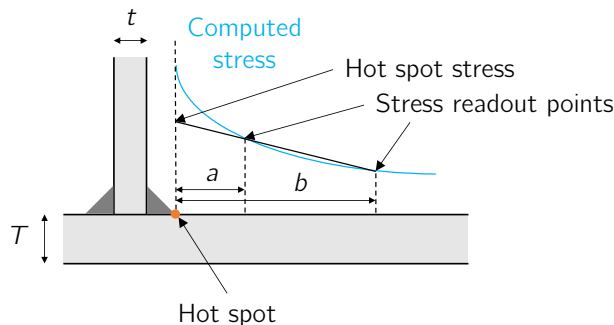


Figure 1.10: Graphical representation of the HSS extrapolation.

To assess the stresses at the readout points, an FE model or a different computational model is necessary.

For tubular joints, the geometry can either be modeled with 2D or 3D elements and the model may or may not include the weld profile. However, more reliable results are obtained by including the weld in the model [1]. Different extrapolation methods exist for the HSS approach, and for tubular joints in jacket structures, the method provided by DNV-RP-C203 [1] is commonly used, as shown in Appendix A.

1.5.3 Effective Notch Stress (ENS)

The Effective Notch Stress (ENS) approach approximates the weld stresses by taking into account the nominal stress, the effect of the structural detail and the effect of the weld profile. When the stress concentration caused by the geometry of the sharp notch is obtained according to the theory of elasticity, the stress is higher than the expected stress concentration resulting from fatigue experiments. The difference originates from the microstructural support effect, which gives strength at sharp notches based on material-specific grain structure, micro-yielding and crack initiation processes [16].

To incorporate the microstructural support effect, the ENS approach was introduced by Neuber in 1968 [17]. The method imposes a fictitious rounded notch, in which the maximum stress equals the average stress along a certain length ρ^* , as illustrated in Figure 1.11.

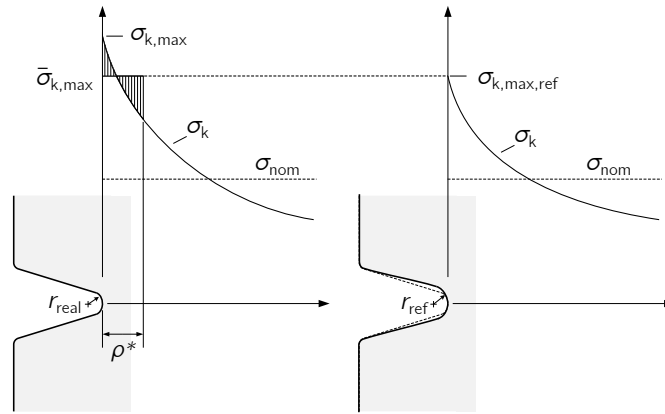


Figure 1.11: The original notch shown on the left-hand side is fictitiously enlarged as shown on the right-hand side, such that the maximum stress equals the average stress around the real notch [10].

The size of the fictitious effective notch radius (r_{ref}), is based on

$$r_{ref} = r_{real} + s \cdot \rho^*, \quad (1.8)$$

with the real notch radius (r_{real}), the multiaxiality coefficient (s) and the microstructural length (ρ^*). For notches in the weld, the worst case is assumed with a real notch radius at the weld toes and root of $r_{real} = 0$. The microstructural support length is found to be negatively correlated to the yield limit and to be in the range of $0.35 \text{ mm} > \rho^* > 0.45 \text{ mm}$ for cast steel [16]. The value of the multiaxiality coefficient depends on the directions of the loading and varies within the range of $s < 3$.

Uniform values of $s = 2.5$ and $\rho^* = 0.4 \text{ mm}$ for notches in steel were proposed by Neuber, resulting in $r_{ref} = 1 \text{ mm}$. An effective notch radius of $r_{ref} = 1 \text{ mm}$ corresponding with S-N curve FAT225 has been widely verified to give consistent results for plates thicker than 10 mm [18][2]. Furthermore, the justification of the FAT225 curve is summarised in Figure 1.12, in which nominal fatigue stresses are shown for different welded joint types and P_s of 90%, 50% and 10%. Significant differences in nominal fatigue strength can be observed between different welded joint types. However, when converting to local principal stresses for a number of load cycles of $N = 2 \cdot 10^6$, modeled with weld toe radii of $r_{ref} = 1 \text{ mm}$, the obtained stress

ranges overlap within a scattered range of $P_s = 10\text{-}90\%$. The average stress range of all the observed local stresses equals:

$$\Delta\sigma_1 = 347 \text{ MPa (with } R = 0, \text{ and } P_s = 50\%). \tag{1.9}$$

Transforming the stress ratio from $R = 0$ to $R = 0.5$ to account for high tensile residual stresses, yields:

$$\Delta\sigma_1 = 316 \text{ MPa (with } R = 0.5, \text{ and } P_s = 50\%). \tag{1.10}$$

Next, reducing the probability of survival from $P_s = 50\%$ to $P_s = 97.7\%$ (mean value minus two standard deviations), results in:

$$\Delta\sigma_1 = 231 \text{ MPa (with } R = 0.5, \text{ and } P_s = 97.7\%). \tag{1.11}$$

Finally, the FAT-value of $\Delta\sigma_1 = 225 \text{ MPa}$ is found by rounding down according to the IIW-numerical system, in which S-N curves are equally spaced at 12.5% intervals [11].

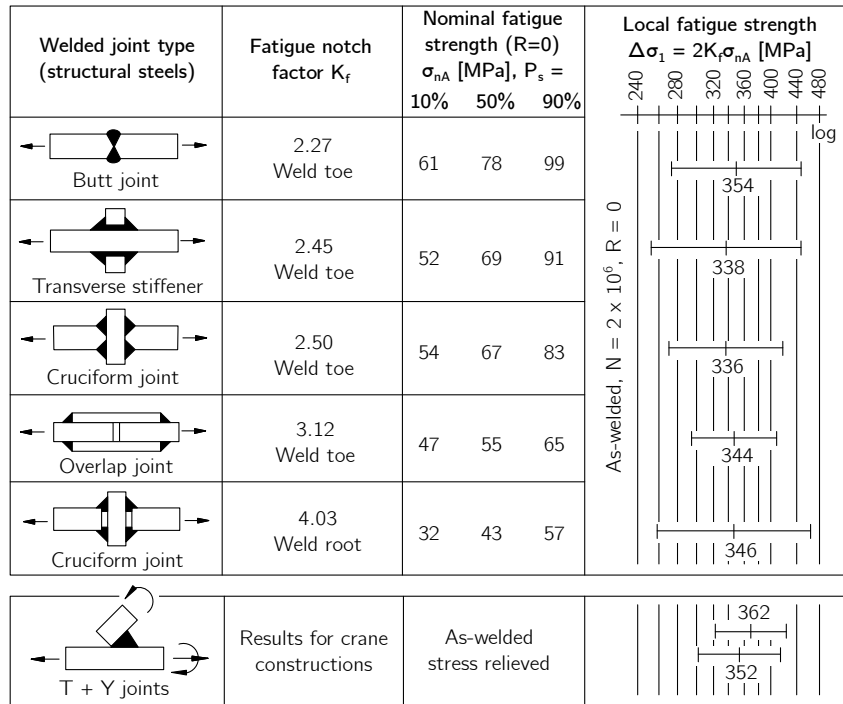


Figure 1.12: Derivation of the FAT225 curve for the ENS approach with $r_{ref} = 1 \text{ mm}$ [11].

For thinner plates, a value of $r_{ref} = 0.05 \text{ mm}$ is most commonly used, which corresponds with the FAT630 S-N curve. The value is based on the relationship between the stress intensity factor and the notch stress, originating from fracture mechanics instead of the theory of elasticity.

Tubular joints in jacket structures are considerably thicker than 10 mm. Therefore, an effective notch radius of $r_{ref} = 1 \text{ mm}$ is used throughout this thesis, with the exception of an investigation on the relationship between the stress and the r_{ref} , shown in Appendix B. For the implementation of the ENS approach, the FE method is commonly used, with the requirement of a very fine mesh. DNV [1] requires a minimum of 4 elements along a quarter of the circle circumference in the effective notch radius, resulting in an element

size smaller than: $\pi/8 \approx 0.39$ mm. IIW [2] requires an element size smaller than 0.25 mm around the notch. Both DNV [1] and IIW [2] recommend quadratic elements and a gradual mesh refinement towards the notch area. Then, the maximum principal stress is evaluated at the effective notch radius, which can be related to a number of load cycles for fatigue failure using the S-N curve. A summary of the approach is presented in Figure 1.13.

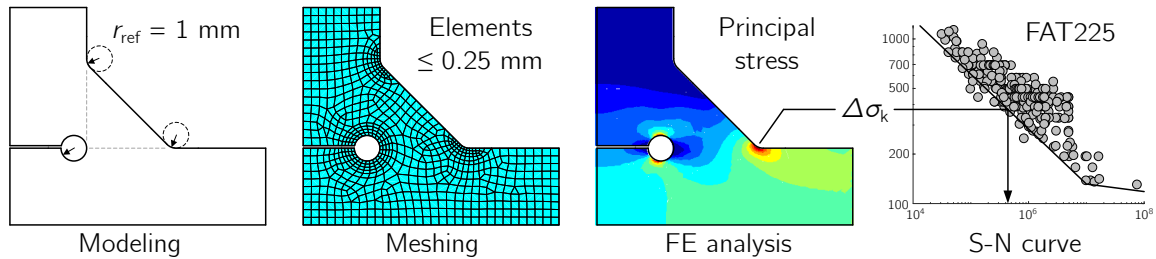


Figure 1.13: The principle of the ENS approach with $r_{ref} = 1$ mm [10].

In the ENS approach, the notch stress is evaluated directly from the FE model without interpolation and thus takes into account the effect on the stress concentration of the weld geometry. Therefore, the approach is typically more accurate, allowing for a less conservative fatigue life estimation.

Principal stress

The principal stress acts in the direction at which no shear stress is present. Therefore, the maximum principal stress is the largest stress value developed on a body, as shown in Figure 1.14.

Figure 1.14: Graphical representation of the normal and shear stresses (left) and the corresponding principal stresses (right).

1.6 Thesis Objectives and Outline

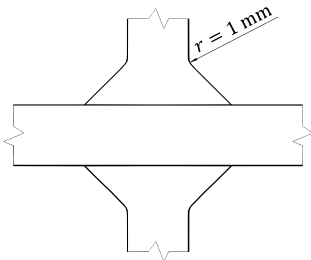
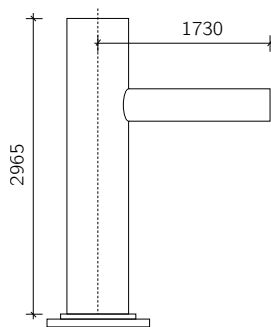
The ENS approach shows the potential to increase the accuracy of the computed fatigue life for welded components. Increasing the accuracy of the computed fatigue life for tubular joints in jacket structures, which are the critical components, means either less steel usage or a longer computed lifetime, which both have a large economic impact on the realisation of offshore wind farms. However, the application of and research on the ENS approach for tubular joints is limited. Therefore, the main research objective for this thesis reads:

“Investigate the application of the ENS approach on a tubular joint.”

To achieve the thesis objective, the research is divided into three parts, each presented in its own chapter, as shown in Table 1.2. The first part of the research focuses on the FE mesh for the ENS approach, as

the accuracy of the results relies upon an adequate FE mesh. Specifically, a cruciform joint example is considered, following the validation procedure outlined in DNV-RP-C203 [1]. Secondly, a study on sub-modeling of the ENS approach is presented, as sub-modeling is currently necessary to make the approach computationally feasible for designing tubular joints. Thirdly, a comparison between the ENS approach and the HSS approach is made to determine if the ENS approach yields an improved fatigue life for a tubular joint. As the HSS approach only considers fatigue failure at the weld toe, weld root failure is considered to be out of the scope of this thesis. Furthermore, both the second and third parts of the research are conducted on a tubular T-joint, as it was part of a fatigue experiment. Finally, overall conclusions and recommendations for further research are presented in chapter 5.

Table 1.2: Thesis outline and objectives.

<p style="text-align: center;">Cruciform joint</p> 	<p style="text-align: center;">FE Mesh for the ENS Approach</p> <ul style="list-style-type: none"> • Investigate how the computational efficiency can be optimised while the accuracy is maintained. • Investigate the accuracy of guideline recommendations. 	<p style="text-align: center;">chapter 2</p>
<p style="text-align: center;">Tubular T-joint</p> 	<p style="text-align: center;">Sub-Modeling for the ENS Approach</p> <ul style="list-style-type: none"> • Investigate how the computational and modeling efficiency can be optimised while the accuracy is maintained. • Investigate the accuracy of sub-modeling. 	<p style="text-align: center;">chapter 3</p>
	<p style="text-align: center;">Fatigue Life Comparison of the HSS and the ENS Approach</p> <ul style="list-style-type: none"> • Compare and investigate the accuracy. • Compare the computed fatigue life. 	<p style="text-align: center;">chapter 4</p>

2 FE Mesh for the ENS Approach

The ENS approach relies upon an adequate FE mesh around the effective notch. Due to the high stress concentrations that originate from the small notch radius, results are sensitive to a poor mesh. In this chapter, a study on the FE mesh of the ENS approach is presented, including the research objectives, methodology, results, discussion and conclusions.

2.1 Research Objectives

The main objectives for the FE mesh study are as follows:

- **Investigate how the computational efficiency can be optimised while the accuracy is maintained.**
Generally, refining a numerical model increases its accuracy, but also increases its computational cost. Therefore, accuracy and computational efficiency are two conflicting objectives. The ENS approach requires a fine mesh, resulting in a large computational model, which subsequently requires large computational costs. Therefore, this research aims to maximise computational efficiency while maintaining sufficient accuracy.
- **Investigate the accuracy of guideline recommendations.**
As discussed in subsection 1.5.3, DNV [1] and IIW [2] require a maximum element size in the notch area of 0.39 mm and 0.25 mm, respectively. This research aims to investigate the accuracy of both guidelines' recommendations.

2.2 Methodology

This research is limited to the application to weld toe failure, in line with the scope of this thesis. To achieve the research objectives, a single geometry of a cruciform joint was selected for FE calculations, in accordance with the validation of methodology specified in DNV-RP-C203 appendix E [1], see Figure 2.1a.

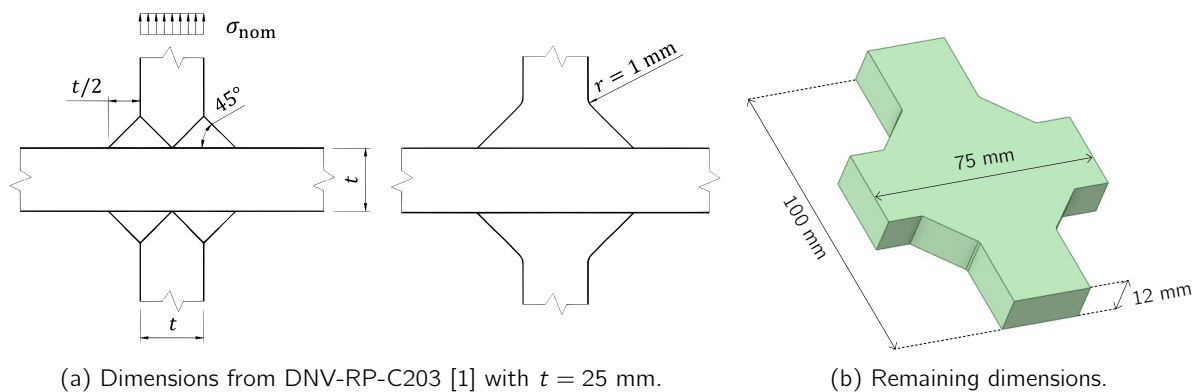


Figure 2.1: Cruciform joint geometry for mesh validation.

In DNV-RP-C203 appendix E [1], the thickness of both plates is specified to be 25 mm. The plate lengths and height are not specified, and dimensions were selected as shown in Figure 2.1b. For the plate at which the effective notch is imposed, a plate length of 100 mm was chosen to have sufficient length for the elements to gradually increase in size towards a constant element size near both ends of the plate. The plate in the transverse direction is further away from the notch and therefore has a smaller length. A relatively small height of 12 mm was chosen compared to the plate thickness, in order to minimise the mesh size of the model. However, the specimen height still allows having multiple elements of 3 mm, which is

the largest element size in the model, along the height. Additionally, the stress gradient along the height is low due to the uniform axial loading, causing the height of the model to be of minor importance.

A uniform axial loading of $\sigma_{nom} = 1$ MPa was applied to one end of the plate and the opposite end of that plate is completely fixed. No gravity was applied and the maximum principal stress was read from the effective notch area, of which the value equals the SCF, see Equation 1.6.

The main area of importance of the FE mesh is around the effective notch radius. To appropriately investigate the FE mesh accuracy, two mesh variants are considered for the effective notch area: the 'rainbow' mesh and the 'ice cream' mesh. These variants are inspired by meshing approaches used by researchers Toor [18] and Baumgartner [19] respectively. Both variants are shown in Figure 2.2 for varying element sizes. The different colours visible in the mesh, represent the bodies used to guide the mesh. For simplicity, the body sizes and shapes are unchanged for the different element size configurations.

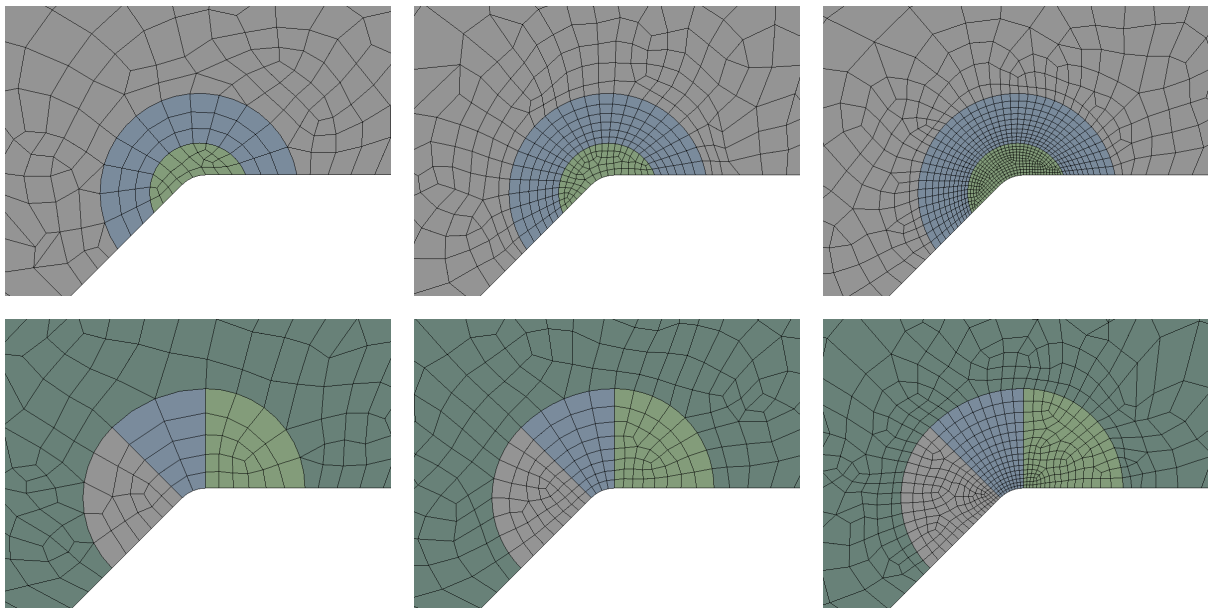


Figure 2.2: Notch area of mesh variants 'rainbow' (above) and 'ice cream' (below) for different element sizes.

Quadratic elements are used and the mesh is configured to majorly exist of hexahedral elements. In this research, the mesh size in the effective notch is decreased from 0.39 mm to 0.07 mm, by increasing the number of elements in the notch by one, from 2 to 11 respectively. The elements are configured to gradually increase in size from the effective notch to a uniform element size of 3 mm, as shown in Figure 2.3.

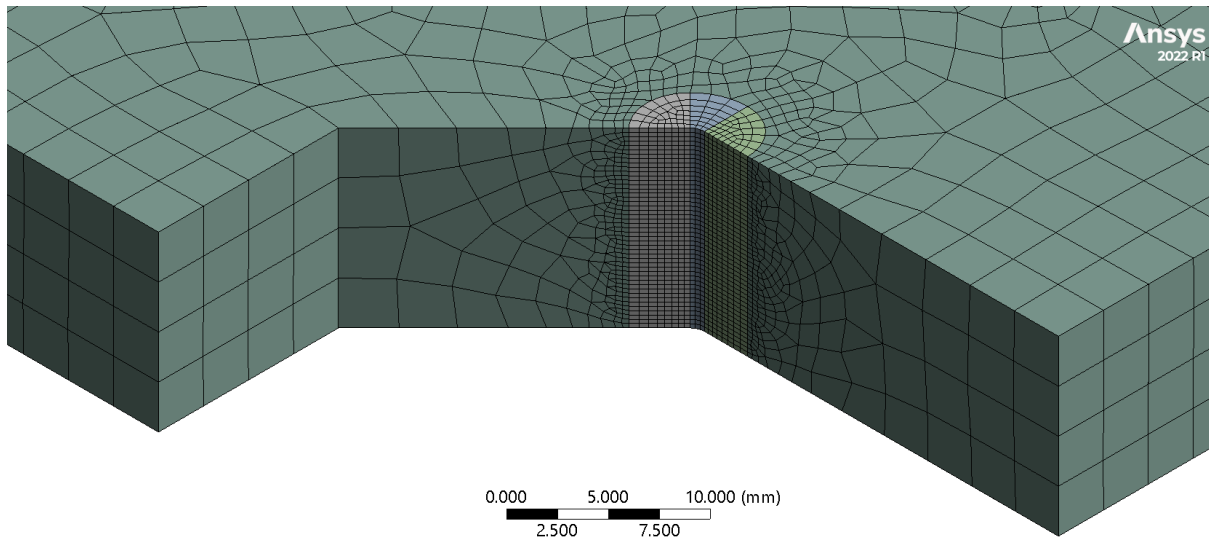


Figure 2.3: 3D representation of the 'ice cream' mesh with a notch element size of 0.26 mm.

2.3 Results and Discussion

Both the averaged and unaveraged maximum principal stress values are evaluated for all models. In Figure 2.4, the location at which the maximum (averaged) principal stress occurs in the model is shown. During analysis of the results, it was observed that both the averaged and unaveraged maximum principal stresses occur at the same location along the weld for all models.

Averaged and unaveraged stress

In the FE method, adjacent elements do not share nodes, which leads to situations where two or more nodes from different elements exist at the exact same location in the model. These nodes share the same displacements but can have different stress values, as the strains that lead to the stresses are solved for the elements independently. The averaged stress refers to the average of all stress values for each node located at the same position. On the other hand, the unaveraged stress can have different values at the same location.

All obtained maximum principal stress values, which are equal to the SCF, are plotted as a function of the element size in the notch, as shown in Figure 2.5. The figure includes the recommended maximum element sizes in the notch by DNV [1] and IIW [2], represented by dashed lines. Convergence can be observed towards a value of 3.31 for both the 'rainbow' mesh and the 'ice cream' mesh, as well as for the averaged and unaveraged stress values. The DNV-RP-C203 [1] validation methodology recommends finding an SCF close to 3.17. The discrepancy with the obtained converged SCF can be explained by the plate lengths and height of the specimen, which are not given by the guideline, but do influence the SCF.

Compared to the notch element size, the 'rainbow' mesh shows a better convergence behaviour than the 'ice cream' mesh. The reason for the 'ice cream' mesh to perform better could be explained by the consistent element size and the higher density of elements near the notch area. Moreover, an oscillating SCF can be observed for both variants, which can be attributed to the fact that one element is added in the notch for each decrease in element size, causing the location of maximum principal stress to shift. Furthermore, for relatively large element sizes the 'rainbow' mesh overestimates the SCF, while the 'ice cream' underestimates it. This difference may be attributed to the orientation and aspect ratio of the elements in the notch. The longer sides of the elements in the 'rainbow' mesh are parallel to the specimen edge, whereas in the 'ice

'cream' mesh, they are perpendicular to the edge.

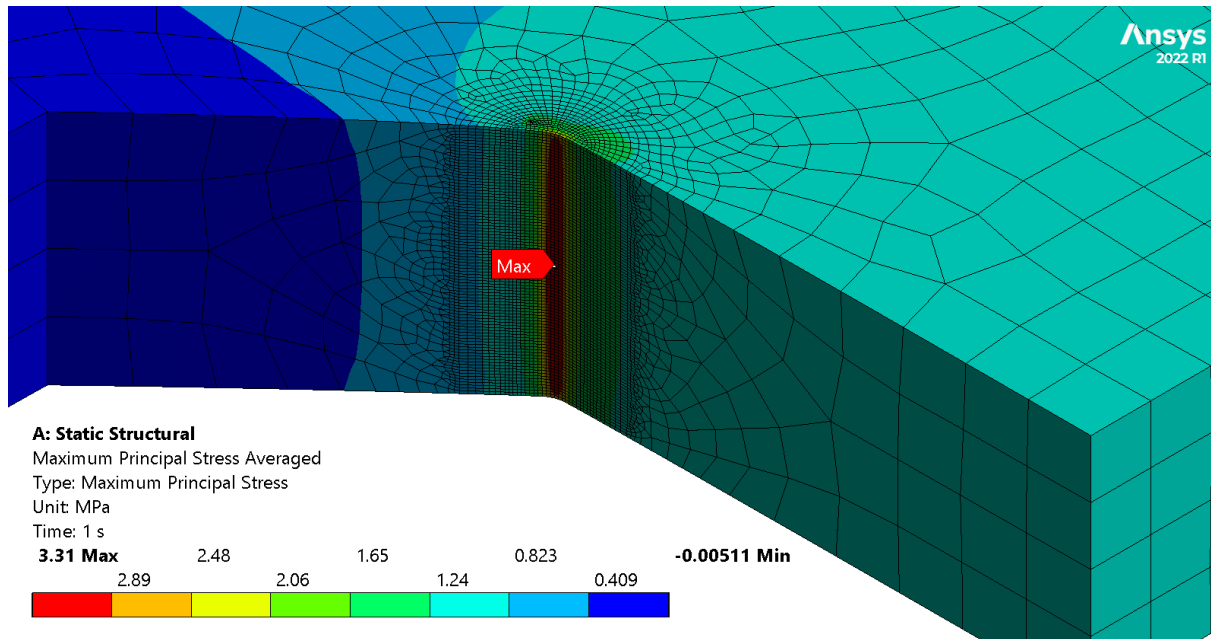


Figure 2.4: Maximum averaged principal stress for 'rainbow' mesh with a notch element size of 0.20 mm.

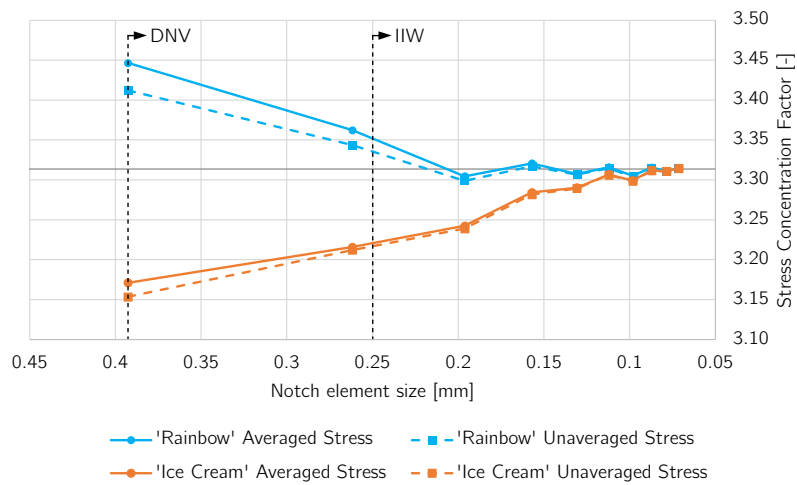


Figure 2.5: SCF versus the notch element size.

In the way both mesh variants are configured, the 'rainbow' mesh needs a larger number of nodes for the same element size in the notch, as shown in Figure 2.6. This can be explained by the fact that the 'rainbow' mesh has a constant element size in the area around the notch, in Figure 2.2 depicted in green, while for the 'ice cream' mesh the element size increases gradually from the notch. Especially for the finer mesh configurations, mesh size optimisation could be achieved by decreasing the area of constant element size around the notch, but is considered to be out of the scope of this thesis. The question that arises is which mesh variant demonstrates better convergence behaviour in relation to mesh size. Therefore, the SCF is plotted as a function of the mesh size and is shown in Figure 2.7.

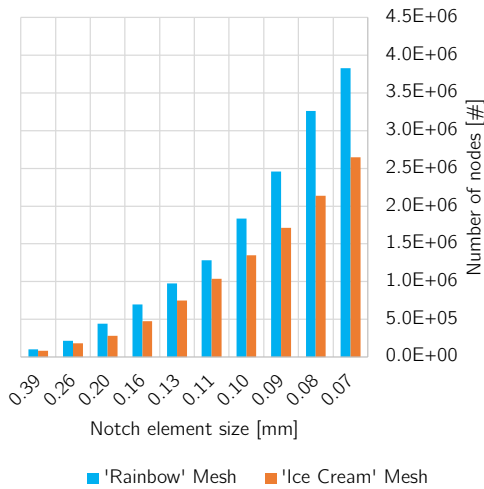


Figure 2.6: Mesh sizes.

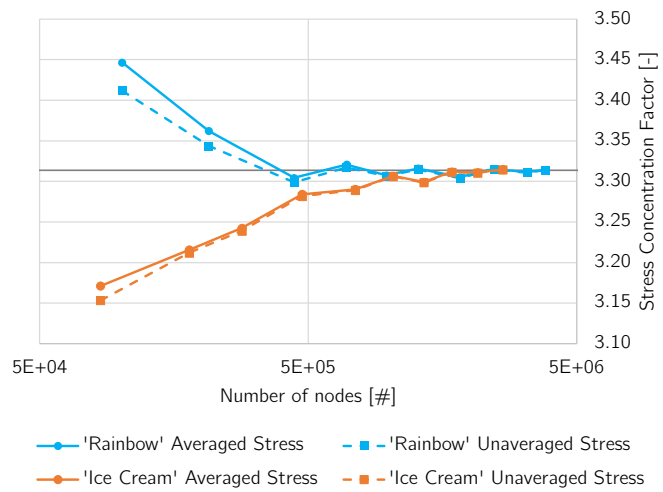


Figure 2.7: SCF versus the mesh size.

Compared to the mesh size, both mesh variants lie closer to each other in terms of SCF convergence behaviour. This indicates that there is a stronger positive correlation between the accuracy of the mesh and the number of nodes surrounding the notch than there is between the accuracy of the mesh and the element size in the notch. Even though the convergence behaviour of both mesh variants is closer related to the number of nodes, the 'rainbow' mesh still performs better.

An overview of the results is presented in Table 2.1, with δ being the relative error compared to the converged SCF value of 3.314. The errors of 3.99% and -4.32% obtained with the recommended maximum element size of 0.39 mm by DNV-RP-C203 suggest that these guidelines are not valid. The discrepancy of approximately 8% between the two mesh variants further supports this conclusion. However, it should be noted that the guideline recommends validating the meshing approach using the specific geometry considered in this research to achieve an SCF close to 3.17. This means that one could use the 'ice cream' mesh with element sizes in the notch of 0.39 mm and consider the approach validated, while having stress errors of around 4%. It is important to highlight that there is an exponential relationship between the number of load cycles and the stress range. Therefore, a 4% error in SCF results in a difference in number of load cycles of approximately 12% and 22% in the low and high cycle fatigue regimes, respectively.

Regarding the recommendation of a maximum element size of 0.25 mm by IIW, a maximum error of -2.17% is achieved with the 'ice cream' mesh. Notably, a discrepancy of approximately 2% was observed between the two mesh variants following the guideline. Similarly, the exponential relationship between the number of load cycles and the stress range implies that a 2% discrepancy in SCF results in a difference in number of load cycles of approximately 6% and 10% in the low and high cycle fatigue regions, respectively.

Although relative errors of 1.45% and -2.17% for the 'rainbow' and 'ice cream' meshes, respectively, can be considered as sufficiently accurate for design purposes, a higher standard is maintained for further research in order to minimize the influence of meshing errors. Consequently, the mesh configuration with a relative error of 0.29% has been selected, highlighted in grey in Table 2.1. This configuration is considered highly accurate and is achieved without significantly increasing the mesh size.

Table 2.1: Mesh study results. The selected mesh configuration for further research is highlighted in grey.

Notch element size [mm]	Number of nodes in notch [#]	'Rainbow' mesh			'Ice cream' mesh		
		SCF averaged stress [-]	δ averaged stress [%]	Number of nodes in mesh [$\cdot 10^3$]	SCF averaged stress [-]	δ averaged stress [%]	Number of nodes in mesh [$\cdot 10^3$]
0.39	2	3.447	3.99	101	3.171	-4.32	84
0.26	3	3.362	1.45	213	3.216	-2.97	180
0.20	4	3.304	-0.29	443	3.242	-2.17	283
0.16	5	3.321	0.20	695	3.284	-0.91	474
0.13	6	3.308	-0.20	977	3.290	-0.72	748
0.11	7	3.316	0.05	1281	3.307	-0.23	1036
0.10	8	3.305	-0.27	1835	3.299	-0.46	1349
0.09	9	3.315	0.04	2457	3.312	-0.07	1713
0.08	10	3.311	-0.09	3259	3.311	-0.10	2136
0.07	11	3.314	0.00	3827	3.315	0.01	2647

2.4 Conclusions

The accuracy of different mesh configurations for the ENS approach was evaluated and based on the results obtained, the following conclusions can be made:

- The 'rainbow' mesh model with a notch element size of 0.20 mm is the most suitable, considering the combination of accuracy and mesh size.
- With a maximum notch element size of 0.39 mm, according to DNV [1], unacceptable SCF errors of 4.0% and -4.3% were found for the considered mesh variants with a corresponding discrepancy between both variants of approximately 8%.
- With a maximum notch element size of 0.25 mm, according to IIW [2], SCF errors of -0.3% and -2.2% were obtained for the 'rainbow' and 'ice cream' mesh variant, respectively. Therefore, with a notch element size smaller than 0.25 mm, accurate results can be obtained but are not guaranteed.
- The accuracy of the mesh was found to be primarily influenced by the number of nodes surrounding the notch, rather than the size of the elements in the notch.

3 Sub-Modeling for the ENS Approach

To ensure the computational feasibility of the ENS approach for designing tubular joints, it is currently necessary to use a sub-modeling approach in which only a fraction of the weld area is modeled according to the ENS approach. In this chapter, a study on sub-modeling the ENS approach for a tubular joint is presented, including the research objectives, methodology, results, discussion and conclusions.

3.1 Research Objectives

The main objectives for this research on sub-modeling of the ENS approach on a tubular joint are as follows:

- **Investigate how the computational and modeling efficiency can be optimised while the accuracy is maintained.**

This study investigates the effect of different modeling choices, including the global model element type (2D vs 3D), the weld profile in the global model, and the sub-model size, on the performance in terms of modeling effort, computational cost and accuracy. To reduce modeling effort, 2D elements can be used and the weld profile can be excluded from the global model. To reduce the computational cost, 2D elements can be used for the global model and the sub-model size can be decreased. However, where modeling effort and computational cost are reduced, a corresponding decrease in sub-modeling accuracy can be expected. Therefore, this study aims to find a balance resulting in the best-performing sub-modeling approach.

- **Investigate the accuracy of sub-modeling.**

The potential loss of accuracy due to sub-modeling for the ENS approach is not found to be discussed in literature. Commonly, a global model is created that closely matches the geometry of the sub-model and validation methods can be used to evaluate the sub-modeling approach. However, small errors resulting from the displacement coupling at the sub-model boundaries are typically considered negligible. This research aims to investigate this potential error by comparing the sub-modeling results to those obtained from a global model where the ENS approach is applied.

3.2 Methodology

This research is conducted on a tubular T-joint representing the global model and a fraction of the weld area of that T-joint representing the sub-model, where the ENS approach is applied. The global model is loaded on the brace end and the boundaries of the sub-model are connected to the global model through the coupling of displacements.

To measure the accuracy of sub-modeling, a global model is created as a reference, where the ENS approach is applied to the full weld circumference of the T-joint. This model is referred to as the 'ENS Global Model'. To investigate how the choice for 2D or 3D elements and the type of weld profile for the global model affect the accuracy of sub-modeling, five additional global models are created. Each of these models provides boundary conditions for the sub-model, and the maximum principal stresses obtained from the sub-models are compared to those obtained from the 'ENS Global Model'. To investigate how the sub-model size affects the accuracy of sub-modeling, different sizes have been tested. An overview of the methodology is presented in Figure 3.1.

Further details on the global models and sub-models are presented in subsection 3.2.1 and subsection 3.2.2, respectively.

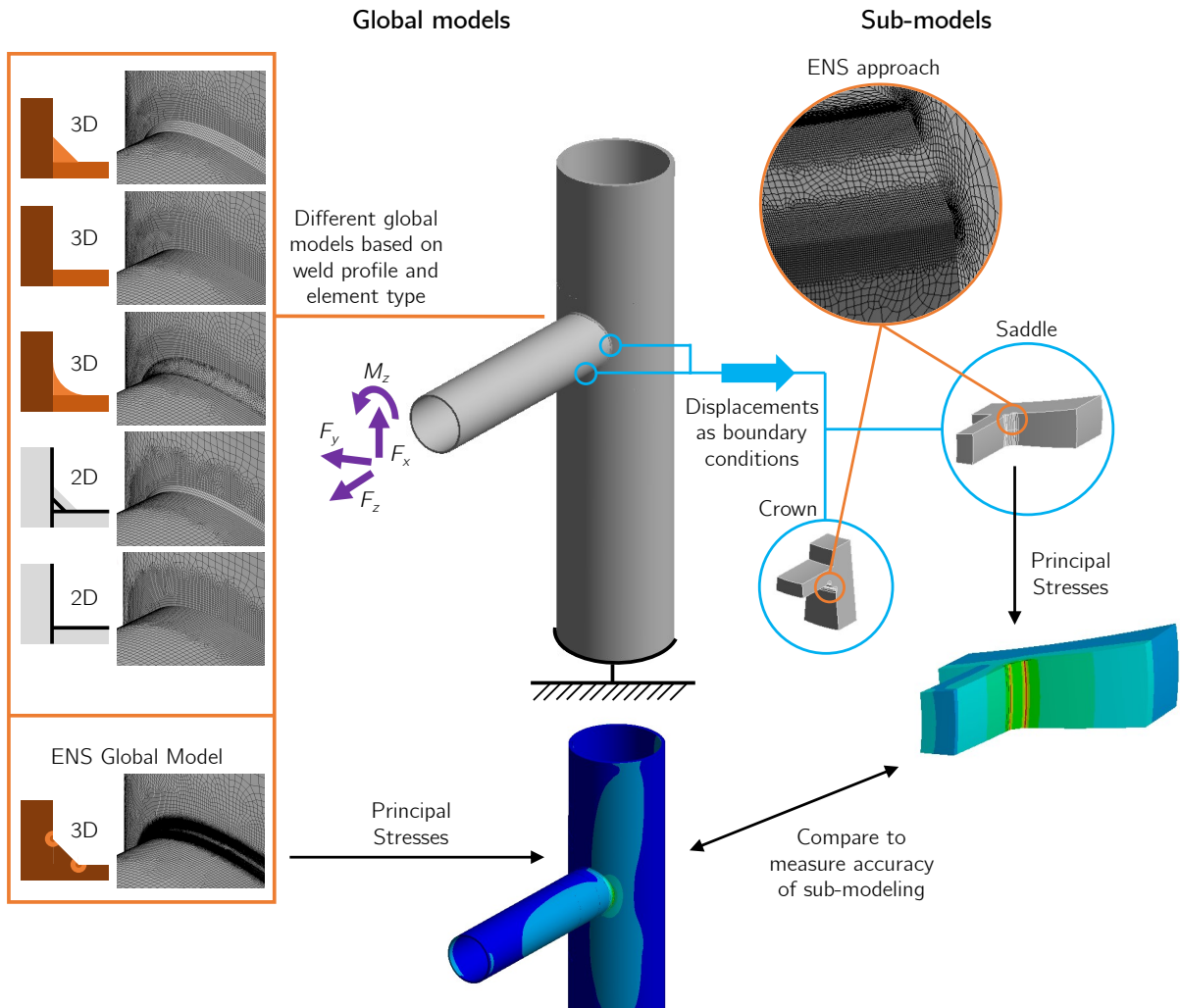


Figure 3.1: Overview of the methodology for the sub-modeling study.


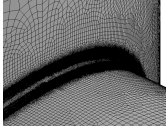

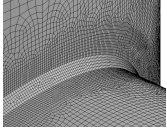

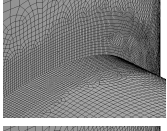
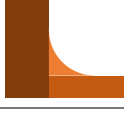
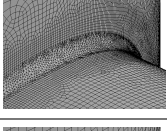
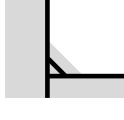
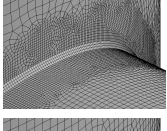

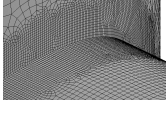
3.2.1 Global Model Parameters

The selected tubular joint geometry for the global model, represents the T-joint of a fatigue experiment which is further elaborated on in chapter 4. A picture of the experimental setup and the dimensions of the T-joint are presented in Figure 4.1. This subsection elaborates on the FE mesh and weld profiles of the considered global models and their boundary conditions.

FE Mesh and Weld Profiles

In total six global FE models of the T-joint are tested for sub-modeling and they differ in element type (2D/3D) and weld profile. The 'ENS Global Model' serves as the reference model to compare the sub-model results with, but is also used for sub-modeling, as a validation of the approach. A summary of the characteristics of the six considered models is listed in Table 3.1 and a motivation for including each of the models is given below.

Table 3.1: Characteristics of the used global models.

Model name	Element type	Weld profile		Number of nodes [#]	Number of elements [#]
ENS Global Model	3D			24,000,000	6,400,000
Solid Chamfer Weld	3D			1,500,000	430,000
Solid No Weld	3D			1,500,000	430,000
Solid Rounded Weld	3D			1,500,000	430,000
Shell Chamfer Weld	2D			150,000	50,000
Shell No Weld	2D			150,000	50,000

- The 'ENS Global Model' serves as a reference to compare the sub-modeling results with and is also used for sub-modeling validation. The weld profile is represented as a chamfer since the ENS approach requires a sharp corner to impose the effective notch radius.
- The 'Solid Chamfer Weld' is expected to be the most suitable for sub-modeling as it has the same geometry as the 'ENS Global Model' except for the effective notch radius.
- The 'Solid No Weld' requires less modeling effort, compared to the 'Solid Chamfer Weld', and is also included to make a fair comparison on the effect of element type on the accuracy of sub-modeling, by comparing with the 'Shell No Weld' model.
- The 'Solid Rounded Weld' is included because its mesh is validated against the experimental data as shown in Appendix F, and to investigate the effect on the accuracy of sub-modeling by using a weld profile different from the sub-model.
- The 'Shell Chamfer Weld' requires less computational costs compared to the models composed of 3D elements and is expected to be the most suitable for sub-modeling when using 2D elements because of its matching geometry with the sub-model.
- The 'Shell No Weld' requires less computational costs compared to the models composed of 3D elements and requires the least modeling effort.

The element sizes of the mesh are consistent for all models, except for the weld region of the 'ENS Global Model', where the mesh is configured using the ENS meshing approach presented in chapter 2. For the

remaining models, the mesh is also most refined in the region of the weld, with an element size of 2.0 mm. The element size is gradually increased from the weld region towards an element size similar to the thickness of the brace and chord plate. All elements are of the second order, i.e. quadratic elements were used.

The element sizes were selected based on a mesh convergence study conducted on the 'Solid Rounded Weld' model. The stresses were measured at the HSS extrapolation points along the chord and brace, at distances from the weld indicated in Appendix A. The mesh was refined until the stress values converged, with the resulting stresses for the selected element sizes for the 'Solid Rounded Weld' model being within 0.5% of the converged stress values. Additionally, the corresponding strain values of the 'Solid Rounded Weld' model were compared to the measured strains from the experimental model, and a good correlation was observed, as shown in Appendix F.

Boundary Conditions

The T-joint is fully constrained at the lower chord end and loads are applied at the brace end, in line with the experiment. Four load cases are considered to account for potential differences in sub-modeling accuracy due to load type and direction. The load cases include an in-plane force (F_x), an out-of-plane force (F_y), an axial force (F_z) and a torsion moment (M_z), respectively resulting in in-plane bending (IPB), out-of-plane bending (OPB), axial loading (AL) and a torsion moment (TM) at the weld area. The forces have a magnitude of 10 kN, while the torsional moment has a magnitude of 10 kNm.

3.2.2 Sub-Model Parameters

The sub-model represents a fraction of the weld area of the T-joint where the ENS approach is applied and equals a fraction of the 'ENS Global Model'. This subsection elaborates on the dimensions, location, FE mesh and the boundary conditions of the sub-model.

Dimensions

Four dimensions can be distinguished for the sub-model size, three dimensions perpendicular to the weld and one dimension parallel to the weld. Varying all dimensions independently for sub-model calculations is a time-consuming process. Moreover, the dimensions perpendicular to the weld have a minor influence on the mesh size and the corresponding boundaries are located where the stress gradients are significantly lower. Additionally, the mesh size is critical for the computational cost of the sub-modeling approach. Therefore, the dimension parallel to the weld is regarded as the most critical parameter of the sub-model size and is the only varied dimension throughout this sub-modeling study, expressed as an angle of the brace circumference, as shown in Figure 3.2b. The considered sub-model sizes are listed in Table 3.2.

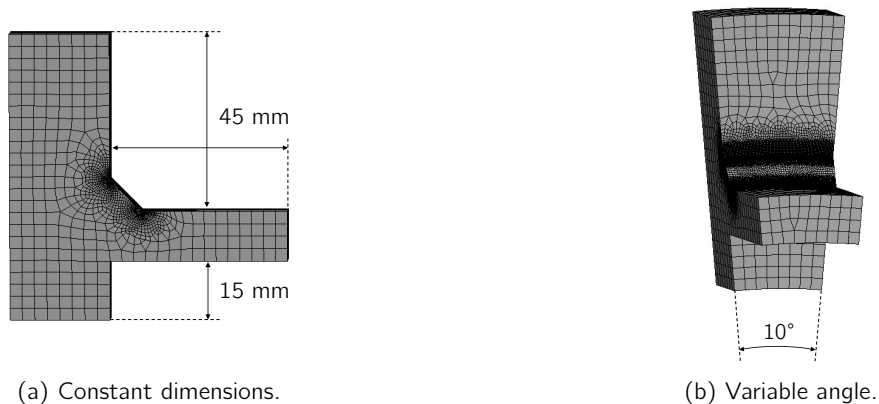


Figure 3.2: Sub-model dimensions.

To determine appropriate lengths for the three dimensions perpendicular to the weld, the displacements near the weld were investigated for all considered global models. The results are presented and discussed in Appendix C and dimensions are selected as shown in Figure 3.2a.

Locations

The sub-models are located at the crown and saddle points of the T-joint, because these points experience the highest stress concentrations as a result of the applied loads at the brace end.

FE Mesh

The sub-model FE mesh is configured according to the approach presented in chapter 2 and the mesh statistics for the different sub-model sizes are listed in Table 3.2.

Table 3.2: FE mesh statistics for the sub-models.

Sub-model size [°]	Number of nodes [#]	Number of elements [#]
30.0	1,870,000	500,000
20.0	1,220,000	330,000
10.0	570,000	150,000
6.67	330,000	87,000
3.33	170,000	45,000
1.67	95,000	25,000
0.83	45,000	11,000

Boundary Conditions

The displacements from the global models are coupled to the full boundary surfaces of the sub-models. With the exception of the 'ENS Global Model' and the 'Solid Chamfer Weld' model, the boundary surfaces of the global models do not precisely match the geometry of the sub-model, as they do not cover the entire weld profile. When there is no overlap between surfaces, the displacements are extrapolated to provide complete coverage of the boundary surface. The displacements originating from different global models at a boundary surface of the sub-model are shown in Figure 3.3.

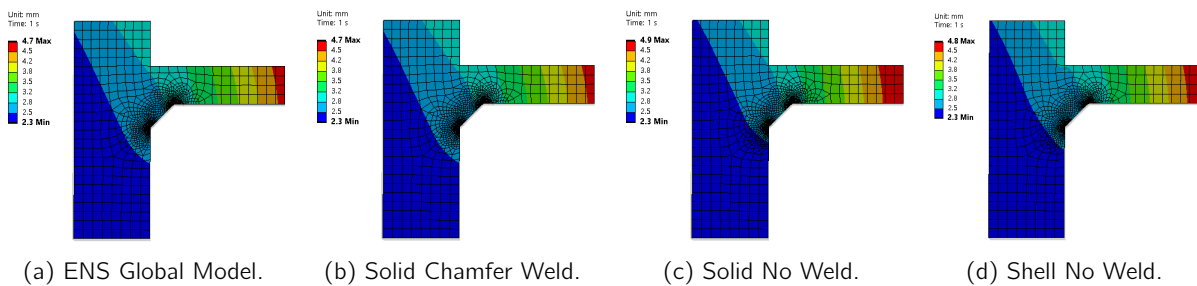


Figure 3.3: Displacements at the sub-model boundary at the crown position for load case F_x , originating from the indicated global models.

3.3 Results and Discussion

To measure the accuracy of the sub-modeling approach, the maximum principal stresses from the sub-models are compared to those from the 'ENS Global Model' at the corresponding location. Shown in Figure 3.4, each graph displays the relative error of the principal stress value at the location of maximum stress for a

specific load case, with the corresponding load case and location of the highest stress indicated above each graph. The x-axes correspond to the sub-model size, while the colour of the data points corresponds to the global model coupled to the boundary conditions of the sub-model. The black line represents the relative error obtained from the sub-model with boundary conditions coupled to the 'ENS Global Model'. This data is used to validate the results and is not easily visible in the graphs because it is overlaid by the blue and purple lines, representing the 'Solid Chamfer Weld' and 'Solid Rounded Weld' models respectively.

From the global models providing boundary conditions for the sub-model, the results allow us to distinguish between consistently and inconsistently performing models. The consistently performing models show little difference in error between the load cases and sub-model sizes and include the 'ENS Global Model', 'Solid Chamfer Weld' and 'Solid Rounded Weld'. While for the inconsistently performing models, large differences in error between load cases can be observed and include the 'Solid No Weld', 'Shell Chamfer Weld' and 'Shell No Weld'.

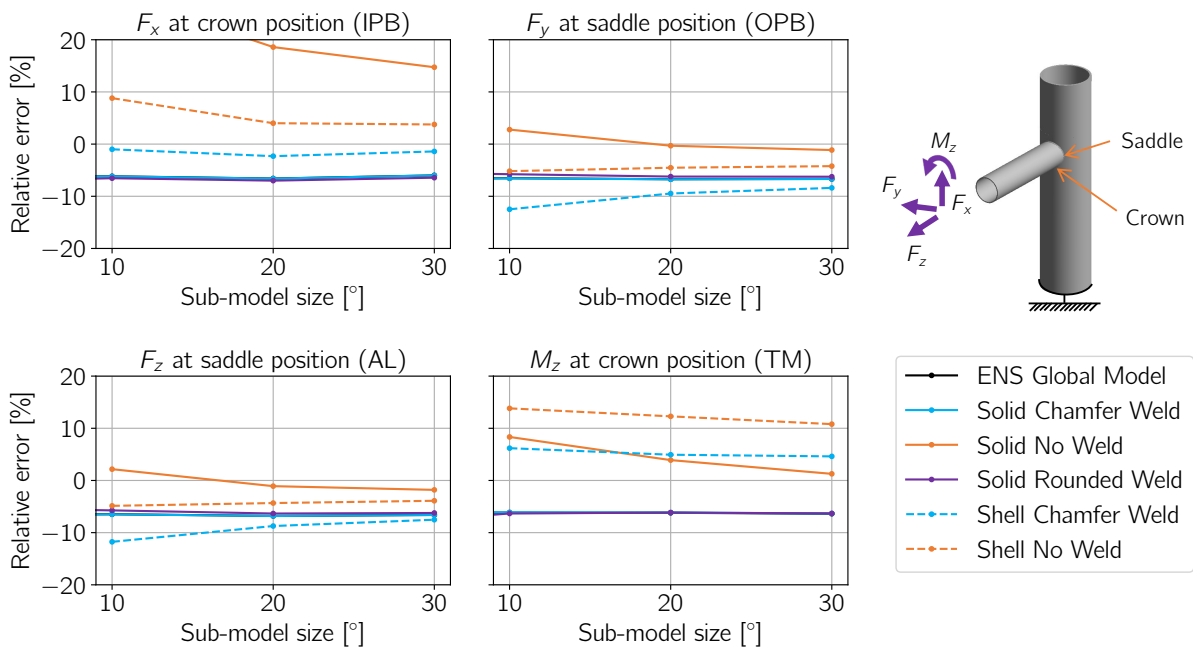


Figure 3.4: The relative error of the sub-modeling approaches for the different sub-model sizes and load cases.

For the consistently performing models, an almost identical error of approximately -6% is observed across all load cases and sub-model sizes. This is an unexpected result, given that the global ENS model has the same geometry and element sizes as the sub-model, suggesting that the error of approximately -6% arises solely from displacement coupling at the boundaries.

The inconsistently performing models show low errors for some load cases but high errors for others. This inconsistency can be explained separately for the use of 2D elements and the exclusion of a weld profile. The 2D elements in the shell models have only one layer of nodes that represents the plate thickness, and thus the displacements along the thickness are not captured accurately. The inconsistency due to the exclusion of a weld profile can be explained by two factors. Firstly, the displacements at the sub-model's weld profile may not accurately represent the actual displacement. This is because the global model displacements are extrapolated along the sub-model's weld profile. Secondly, due to the exclusion of the weld profile, the overall stiffness of the model is different, which leads to inaccuracies in the entire displacement field. One of the coupled sub-model boundaries with different displacement fields was presented in Figure 3.3, showing the discussed inaccuracies.

The inconsistently performing models show lower errors for larger sub-model sizes, which can be explained by two factors that are interrelated. Firstly, the sub-model boundaries are further away from the stress concentration, therefore the stress gradients are lower at the boundaries, which subsequently results in lower errors due to inaccuracies at the boundaries. Secondly, a larger sub-model represents a larger part with correct stiffness, which ensures a better representation of the 'ENS Global Model', resulting in lower errors.

The consistently performing global models were evaluated using smaller sub-model sizes, and the results are shown in Figure 3.5. The graphs reveal that the 'Solid Rounded Weld' model produces inaccurate results for sub-model sizes of 3.33° and smaller. The 'Solid Chamfer Weld' continues to produce consistent results up to the smallest considered sub-model size, except for the torsion moment (TM) load case. Consequently, a minimum sub-model size of 1.67° gives consistent results for all load cases. Therefore, the computational costs of the sub-modeling approach are significantly reduced when comparing the 95,000 + 1,500,000 nodes required for the sub-model and 'Solid Chamfer Weld' model respectively, with the 24,000,000 nodes required for the 'ENS Global Model'. The comparison shows a reduction in the total required number of nodes by a factor of 15. Additionally, hardly any difference is observed between the 'ENS Global Model' and the 'Solid Chamfer Weld', except for sub-model sizes of 3.33° and smaller.

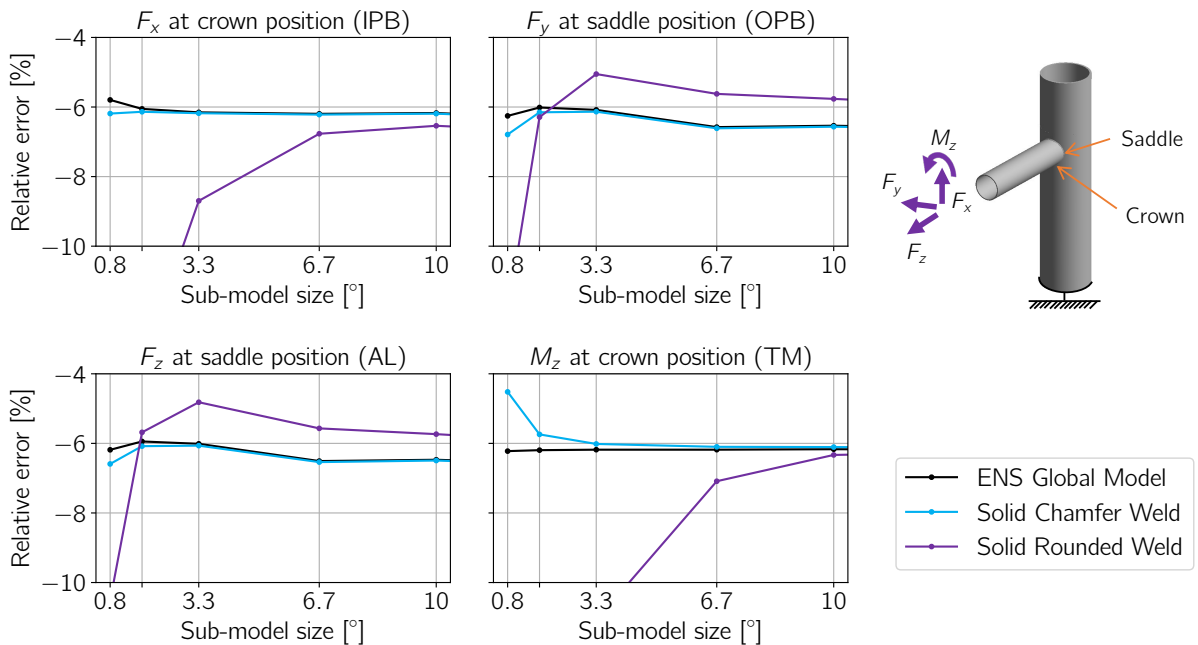


Figure 3.5: The relative error of the consistently performing sub-modeling approaches with smaller sub-models.

The increasing error for smaller sub-models observed in the 'Solid Rounded Weld' model can have a similar explanation as for the 'Solid No Weld' model for larger sub-models. Due to the fact that part of the weld profile's displacement field is extrapolated, and because there is no exact match in stiffness between the sub-model and the global model, the error can be explained. However, since the rounded weld profile matches the sub-model's weld profile more closely than without a weld profile, the 'Solid Rounded Weld' model performs better, although not as well as the 'Solid Chamfer Weld' model.

The error of -6% is consistent for all load cases and sub-model sizes when the boundary conditions are coupled to the 'ENS Global Model' and 'Solid Chamfer Weld' model. In order to investigate the cause of this error, stress and displacements are compared along three paths of the global model and sub-model, as

depicted in Figure 3.6. Load case F_x and the sub-model at crown position coupled to the displacements from the 'ENS Global Model' are considered.

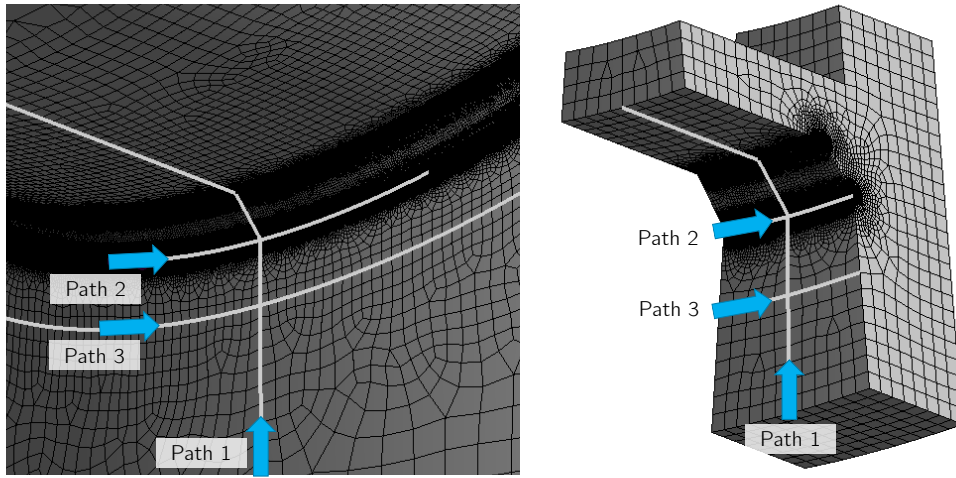


Figure 3.6: The evaluated paths of the global model (left) and the sub-model (right).

In Figure 3.7, the principal stresses and displacements of the global model and the sub-model are plotted for path 1, and the errors of the sub-model relative to the global model are also shown. The same plots are shown for path 2 and path 3 in Figure 3.8.

A consistent relative principal stress error of approximately -6% due to sub-modeling can be observed along all three paths, indicating that this error is present throughout the entire sub-model geometry. Notably, the relative displacement error is approximately 0% along all paths. Additionally, various elements in the global model and sub-model were compared in terms of stresses and displacements. A similar correlation was observed for the elements as for the evaluated paths, as exemplified by the element shown in Figure E.3.

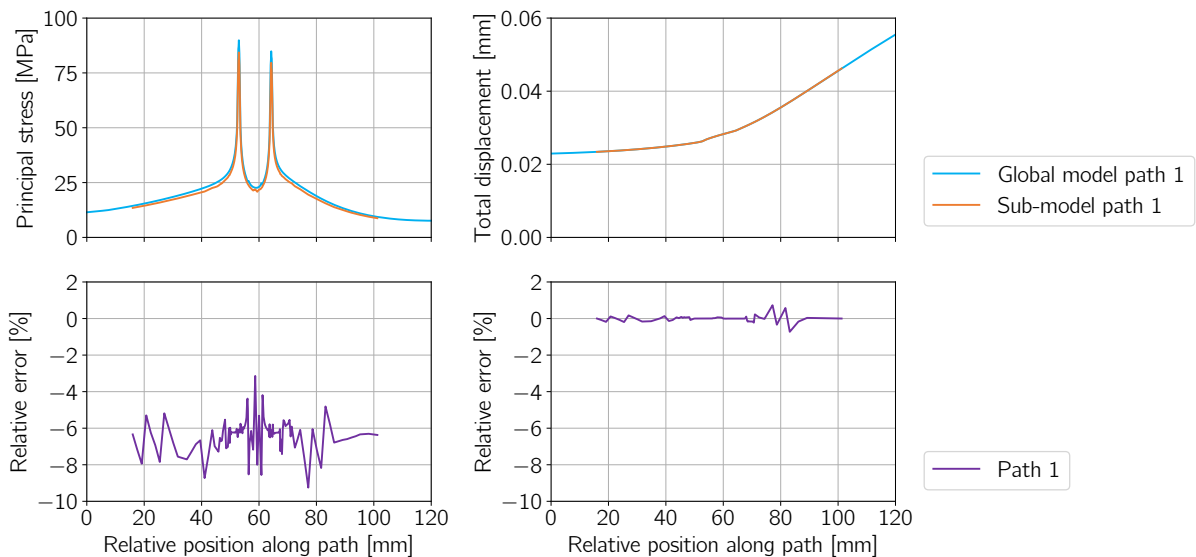


Figure 3.7: The maximum principal stresses (upper left), the total displacements (upper right) and the relative errors of the stresses (lower left) and the displacements (lower right) along path 1.

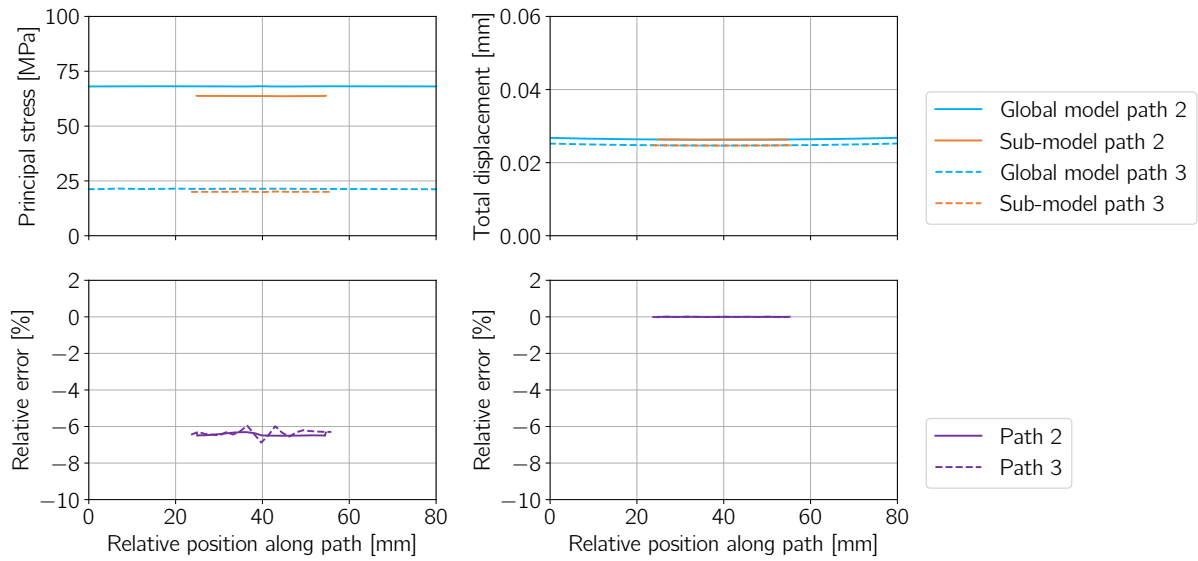


Figure 3.8: The maximum principal stresses (upper left), the total displacements (upper right) and the relative errors of the stresses (lower left) and the displacements (lower right) along paths 2 and 3.

To further investigate the origin of the observed -6% error in sub-modeling, a supplementary study was conducted. In this study, two fictitious welded plates were modeled and a sub-model was made of the weld area. The sub-model boundaries were specifically chosen in regions with low stress gradients, by avoiding boundaries intersecting the effective notch. Further details on this supplementary study can be found in Appendix D. The results show that a stress error of -2% to 2% due to sub-modeling is exclusively present in the effective notch. This suggests that the -6% error found in sub-modeling of the T-joint weld, primarily originates from the boundaries intersecting the effective notch radius.

Apart from the origin of error, it remains odd that there is a negligible error in displacements between the global model and sub-model, while there is an error of approximately -6% in the stresses. This discrepancy becomes even more perplexing when the comparison is made at the elementary level, as shown in Figure E.3. Unfortunately, this phenomenon remains unexplained within the author's current understanding and knowledge.

3.4 Conclusions

The accuracy of sub-modeling for the ENS approach for a tubular T-joint was evaluated by considering different global modeling choices and sub-model sizes. Based on the results obtained, the following conclusions can be made:

- Simplifying the global model by using 2D elements or excluding a weld profile is not recommended, as it leads to inconsistent and inaccurate results. This can be explained by the inaccuracies in the coupled displacement field originating from the simplifications in the global model.
- A global model with a weld profile that does not completely corresponds with the sub-model (referred to as the 'Solid Rounded Weld' model), can give consistent results by ensuring that the sub-model is sufficiently large.
- A global model composed of 3D elements with a weld profile that matches the sub-model (referred to as the 'Solid Chamfer Weld' model), gives consistent results even with small sub-model sizes. In particular, a sub-model size as small as 1.67° of the brace radial angle has been found to give consistent results. When the sub-modeling approach is compared to the global modeling approach, a significant

reduction in computational costs is achieved. This is expressed as a reduction in the required mesh size by a factor of 15. Additionally, a rather surprising error of approximately -6% is observed as a result of sub-modeling for all varied load types and sub-model sizes. The error was found to primarily originate from the sub-model boundaries that intersect the effective notch. Unfortunately, a profound explanation for the magnitude of the error was not found within the author's current knowledge.

4 Fatigue Life Comparison of the HSS and the ENS Approach

This chapter compares the HSS and the ENS approaches for estimating the fatigue life of tubular joints. The ENS approach is typically more accurate and less conservative than the HSS approach, as it takes the stress concentration originating from the weld profile into account. However, the application of and research on the ENS approach for tubular joints is limited. This study aims to determine which approach is more accurate and which approach provides a less conservative fatigue life for tubular joints.

4.1 Research Objectives

The HSS and ENS approaches are compared using different modeling choices. The HSS approach is evaluated with 2D and 3D elements and the inclusion or exclusion of the weld profile in the model. On the other hand, the ENS approach is evaluated with a global model and a sub-modeling approach. The objectives of this research are to compare the accuracy and computed fatigue life of the models:

- **Compare and investigate the accuracy.**

The ENS approach is generally known to be more accurate and less conservative than the HSS approach, but the application to tubular joints is limited. Therefore, this research aims to compare the accuracy of both approaches for a tubular joint. Specifically, by comparing both approaches with data obtained from a fatigue experiment conducted on a tubular T-joint.

- **Compare the computed fatigue life.**

While the HSS approach is typically more conservative, the ENS approach has the potential to reduce design conservatism in tubular joints and thereby provide a longer computed fatigue life for offshore jacket structures. To compare the two approaches, the SCFs are evaluated for various load cases, as the SCFs are the critical components in computing the fatigue life of a tubular joint. However, both approaches use different S-N curves, which are associated with a different type of stress assessment. The ENS approach incorporates the weld profile's stress concentration in the Stress Concentration Factor (SCF), whereas the HSS approach accounts for this effect through the S-N curve. As a result, a direct comparison of the SCFs is not possible. To address this, a Correction Factor (CF) is developed by taking into account both S-N curves, enabling a direct comparison of the two approaches by establishing equivalent SCFs.

4.2 Methodology

This research is divided into two parts, aligned with the research objectives.

1. A comparison with the fatigue experiment to evaluate the accuracy of both approaches, further elaborated on in subsection 4.2.4
2. A comparison of the equivalent SCFs, further elaborated on in subsection 4.2.5.

For both parts of this research, a tubular T-joint is considered and the experimental setup and its properties are introduced first in subsection 4.2.1. To make a profound comparison of the HSS and ENS approach, different FE models are considered for both approaches. Elaboration on these models is provided in subsection 4.2.2. Critical for both parts of this research are the S-N curves linked to both approaches, which are further elaborated on in subsection 4.2.3.

4.2.1 T-Joint Experiment and Properties

To investigate the fatigue life of the T-joint, a single specimen was tested under constant amplitude loading. The experimental setup and the dimensions of the T-joint are shown in Figure 4.1. The loading was applied on the brace end by two actuators and a connection piece. The forces exerted by the actuators are denoted as F_1 and F_2 , and Figure 4.2a depicts the magnitudes of these forces over time. The resulting loads on the brace end are an in-plane force and a torsion moment, denoted as F_x and M_z , respectively. The magnitudes of these loads over time are shown in Figure 4.2b.

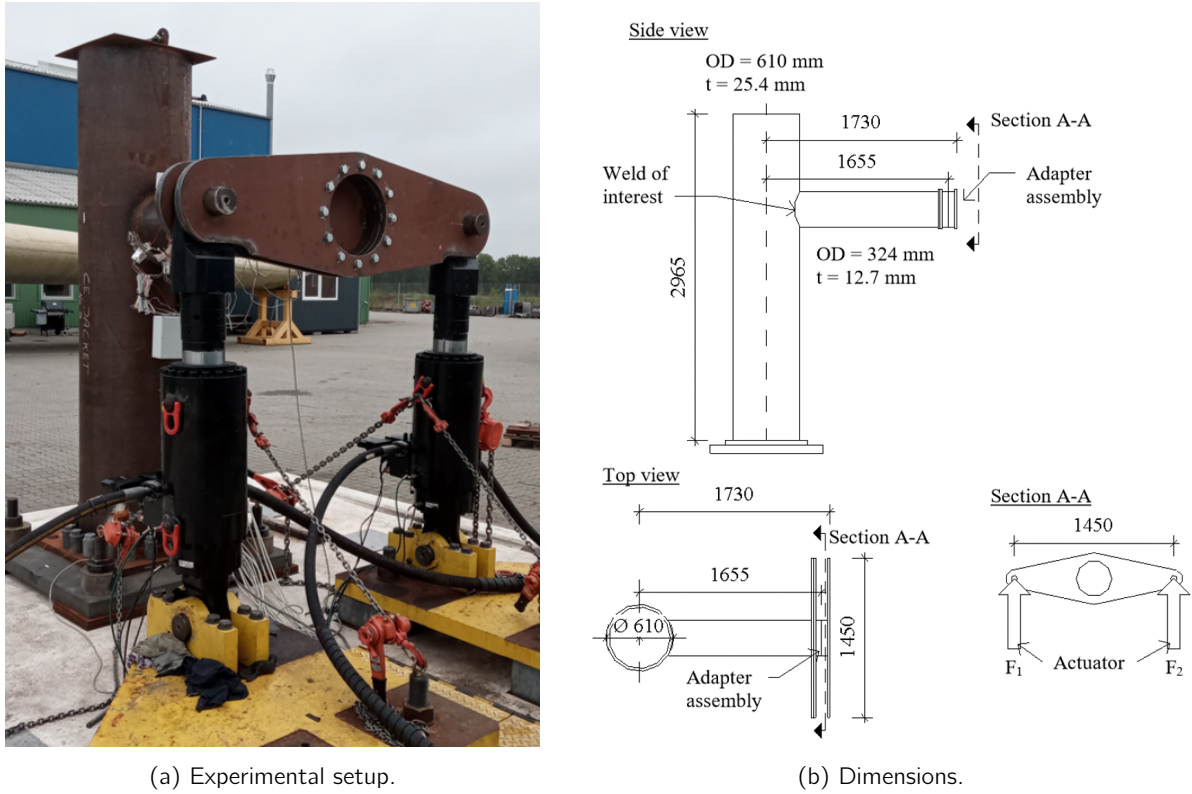


Figure 4.1: The T-joint of the fatigue experiment.

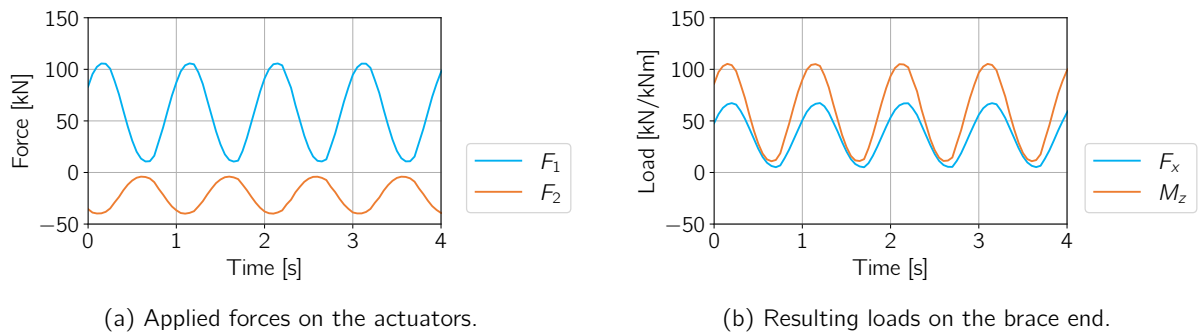


Figure 4.2: Loading of the fatigue experiment.

The T-joint is made of S335 steel with a yield strength of $f_y = 355$ MPa for the brace and $f_y = 345$ MPa for the chord, the yield strength is lower for the chord due to its larger thickness. The Young's modulus of


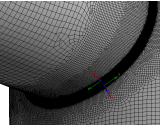

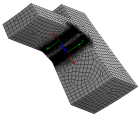

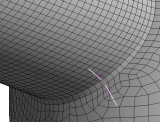

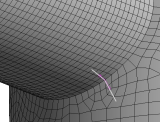
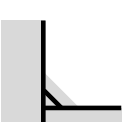
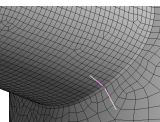
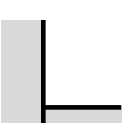
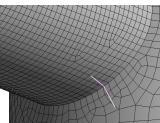
the steel is $E = 210$ GPa and the Poisson's ratio equals $\nu = 0.3$. The exact weld profile of the T-joint was unknown for this research. A weld profile is modeled with leg lengths of 8 mm and these dimensions are based on indicative design drawings.

4.2.2 FE Models

For this research, the FE models of the T-joint only include the two connected tubular beams and the weld profile, without the outer attachments. These models vary in weld profile and element type, in correspondence with the sub-modeling study discussed in chapter 3. However, it's important to note that for the HSS approach, the FE models have a coarser mesh compared to those used in the previous chapter. This is because guidelines DNV-RP-C203 [1] and IIW [20] recommend using element sizes equal to the plate thickness for the HSS approach. By using a finer mesh, the geometrical effect on the stress concentration can be underestimated when extrapolating stresses, as the singularity effect is not properly captured.

The FE models used in this study are listed in Table 4.1. In contrast to the sub-modeling study discussed in the previous chapter, the rounded weld was not considered, as it is difficult to implement with element sizes equal to the plate thickness. This is because the element sizes do not allow for multiple elements in the weld profile, making it hard to create a rounded surface in the FE model. As shown in section 3.3, there is a significant error of approximately -6% due to sub-modeling of the ENS approach. Therefore, both the global and sub-model fatigue results are incorporated in this study. A sub-model size of 10° was selected with coupled displacements from the 'ENS Global Model'.

Table 4.1: Characteristics of the used FE models.

Model name	Element type	Weld profile and stress point/path	Number of nodes [#]	Number of elements [#]
ENS Global Model	3D	 	24,000,000	6,400,000
ENS Sub-Model	3D	 	630,000	170,000
HSS Solid Chamfer Weld	3D	 	110,000	17,000
HSS Solid No Weld	3D	 	110,000	17,000
HSS Shell Chamfer Weld	2D	 	47,000	16,000
HSS Shell No Weld	2D	 	47,000	16,000

4.2.3 The S-N Curves

The S-N curve, which was introduced in section 1.3, is a crucial factor in this research. For the ENS approach, the FAT225 S-N curve is typically used, as discussed in subsection 1.5.3. On the other hand, the HSS approach has a broad set of S-N curves, mainly differing per geometrical detail. In this research, the S-N curve for tubular joints provided by DNV-RP-C203 [1] was used for the HSS approach, also referred to as the T curve.

The S-N curve is typically derived from fatigue tests and design guidelines usually provide the design S-N curve, which serves as a lower bound for the test data. The design S-N curves are utilised for the comparison of the equivalent SCFs, in order to give insights from a design perspective. To have a fair comparison of the HSS and ENS approaches with the experiment, the mean S-N curve obtained from the test data is utilized. The FAT225 S-N curve and the T curve both have their own mean S-N curves, which are discussed in further detail below. The considered design and mean S-N curves and their parameters are listed in Table 4.2.

Table 4.2: Considered S-N curve parameters.

S-N curve	m_1	$\log a_1$	m_2	$\log a_2$
T curve - design	3.0	12.476	5.0	16.127
T curve - mean ($T = 16$ mm)	3.0	12.942	5.0	16.903
T curve - mean ($T = 32$ mm)	3.0	12.681	5.0	16.468
FAT225 - design	3.0	13.358	5.0	17.597
FAT225 - mean	3.0	13.800	5.0	18.333

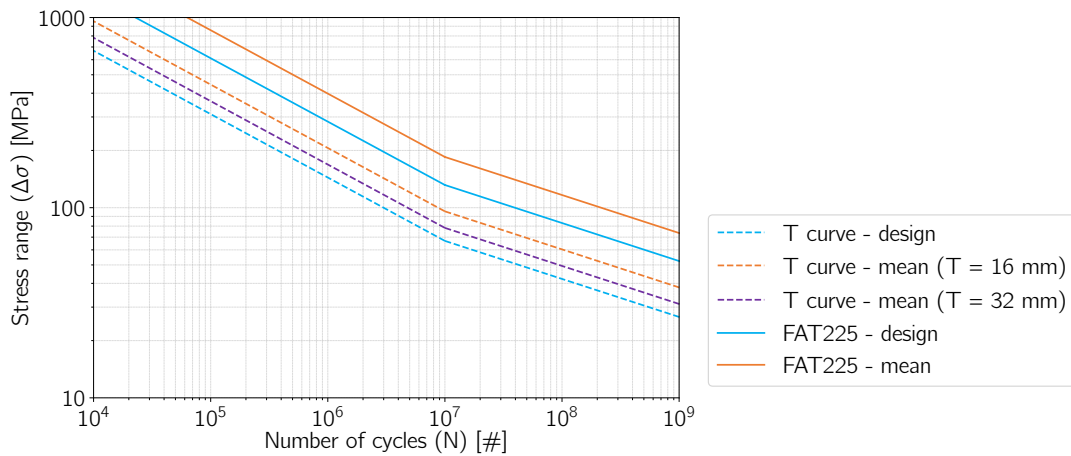


Figure 4.3: Considered S-N curves.

Mean of the T Curve

The derivation of the T curve originates from the fatigue testing of tubular joints, and the results and derivation were published in 1999 [21]. 93 tubular joint specimens were tested, including different geometries and chord thicknesses varying from 16 mm to 90 mm. Predominantly chord thicknesses of $T = 16$ mm and $T = 32$ mm were tested, with brace thicknesses (t) varying from $t/T = 0.5$ to $t/T = 1$. The mean was derived separately for chord thicknesses of $T = 16$ mm and $T = 32$ to fit with a negative slope of $m = 3$ and the results are listed in Table 4.2.

In this study, the fatigue behaviour of the T-joint was evaluated using the mean T curve derived from tests with a reference thickness of 16 mm. However, since the geometry of the considered T-joint falls between

the tested models with $T = 16$ mm and $T = 32$ mm, a thickness effect was considered with a factor of $k = 0.25$, as given by Equation 1.5. The fatigue lives were computed separately for failure at the brace and chord side of the weld. Therefore, the thickness effect was only incorporated for the chord, as the brace thickness is smaller than the reference thickness ($t = 12.7$ mm $<$ $t_{ref} = 16$ mm).

Mean of the FAT225 S-N Curve

The FAT225 S-N curve is derived from a large set of welded plate specimens, as described in subsection 1.5.3. It was found that for different joint geometries, the effective notch stress value could be fitted into one mean S-N curve, with a resistance of 347 MPa for 2 million cycles and a negative slope of $m_1 = 3$. This S-N curve was corrected to a resistance value of 316 MPa to account for high residual stresses. Since the residual stresses in the T-joint are unknown and some residual stresses are expected due to the size of the joint, a resistance value of 316 MPa with a negative slope of $m = 3$ is expected to be the best fit for the mean of the T-joint experiment. The corresponding parameters are listed in Table 4.2.

4.2.4 Comparison With the Fatigue Experiment

To evaluate the accuracy of the HSS and ENS approach, the number of load cycles until failure resulting from the experiment introduced in subsection 4.2.1 was used to compare with the number of load cycles computed with the FE models listed in Table 4.1. To obtain the number of load cycles for failure for all FE models from the resulting loads shown in Figure 4.2b, three steps can be identified. The first step is to identify the critical location for fatigue failure. The second step is to determine the effective stress range at the critical location for all models. The last step is to relate the found effective stress range to a number of load cycles for failure with the corresponding S-N curve. The three steps are elaborated on in more detail below.

1. Identify the critical location for fatigue failure.

To determine the highest effective stress range and corresponding number of load cycles for failure along the weld, steps 2 and 3 were repeated at intervals of 5 degrees for locations around the weld, using the 'HSS Shell No Weld' model. The resulting values are presented in Figure 4.4, where the effective stress and number of load cycles are located on the R-axes, and the location along the weld is located on the θ -axes.

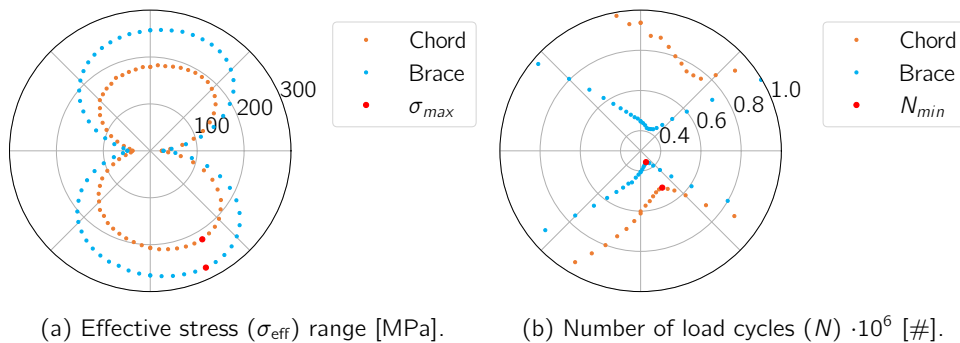


Figure 4.4: Determination of the critical location for fatigue failure using the 'HSS Shell No Weld' model.

As shown in Figure 4.4a, the highest effective stresses occur at 25° and 30° from the bottom for the brace and chord, respectively. To account for the difference in expected failure locations between the chord and brace, as observed in the results shown in Table 4.3, effective stresses were evaluated for all models at an intermediate location of 27.5° from the bottom, for both the brace and chord.

2. Determine the effective stress strange at the critical location for all models.

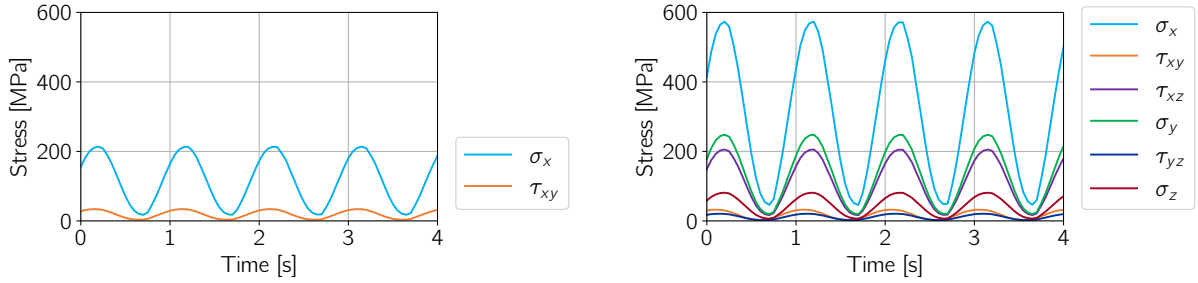
The method of calculating the effective stress is different for the HSS and ENS approaches. In

the HSS approach, the normal and shear stresses are extrapolated linearly from distances away from the weld, as given by Equation A.1 and Equation A.2 for the brace and chord respectively. After extrapolation, the effective stress is obtained using the following equation provided by DNV-RP-C203 [1]:

$$\Delta\sigma_{\text{eff}} = \sqrt{\Delta\sigma_x^2 + 0.81\Delta\tau_{xy}^2}. \quad (4.1)$$

The ENS approach considers all stress components at the effective notch radius and converts them to principal stresses, which then equals the effective stress. The averaged stress components are evaluated at the same node, located in the middle of the effective notch radius.

In both the HSS and ENS approach, the stress components were computed at the critical location as a factor in relation to F_x and M_z using the FE models. By multiplying the obtained factors with the resulting loads on the brace end as a function of time, the stress components as a function of time were computed, as shown in Figure 4.5. Finally, the effective stress was computed as a function of time, from which the effective stress range is taken.



(a) Hot spot stress components resulting from the 'HSS Solid Chamfer Weld' model.

(b) Principal stress components resulting from the 'ENS Global Model'.

Figure 4.5: Stress components at the critical location for failure on the chord side.

- Convert the effective stress range to a number of load cycles for failure.

The effective stress ranges were used to determine the corresponding number of cycles for expected fatigue failure, using the mean S-N curves listed in Table 4.2.

4.2.5 Comparison of the Equivalent SCFs

To gain insights into the relationship between the HSS and ENS approach for tubular joints from a design perspective, the FE models listed in Table 4.1 were subjected to unit loading on the brace end. The loads include an in-plane force (F_x), an out-of-plane force (F_y), an axial force (F_z) and a torsion moment (M_z), respectively resulting in in-plane bending (IPB), out-of-plane bending (OPB), axial loading (AL) and a torsion moment (TM) at the weld area. The forces have a magnitude of 10 kN, while the torsional moment has a magnitude of 10 kNm. The resulting maximum SCFs were compared. However, to make a fair comparison of the SCFs between the HSS and ENS approaches, a CF was introduced based on the design S-N curves. To derive the CF, Equation 1.4 was rewritten for the ENS approach and Equation 1.5 for the HSS method, where the thickness effect is taken into account, resulting in

$$N_{\text{ENS}} = \frac{\bar{a}_{\text{ENS}}}{\Delta\sigma_{\text{ENS}}^m} \quad (4.2)$$

and

$$N_{\text{HSS}} = \frac{\bar{a}_{\text{HSS}}}{\left(\Delta\sigma_{\text{HSS}} \left(\frac{t}{t_{\text{ref}}}\right)^k\right)^m} \quad (4.3)$$

respectively. When the number of cycles is equal between the two approaches ($N_{ENS} = N_{HSS}$), the right-hand side of both Equation 4.2 and Equation 4.3 can be equated and solved for $\Delta\sigma_{ENS}$, resulting in

$$\Delta\sigma_{ENS} = \left(\frac{\bar{a}_{ENS}}{\bar{a}_{HSS}} \right)^{1/m} \left(\frac{t}{t_{ref}} \right)^k \Delta\sigma_{HSS}, \quad (4.4)$$

which includes the CF for the HSS stresses. The reference thickness equals $t_{ref} = 16$ mm, and $t = 16$ mm is taken for the brace as for $t < t_{ref}$ holds that $t = t_{ref}$ and the chord thickness equals $T = 25.4$ mm. With the thickness exponent of $k = 0.25$ and the values of the design S-N curves listed in Table 4.2, the CFs for the brace and chord can be derived, resulting in

$$CF_{brace} = \left(\frac{10^{13.358}}{10^{12.476}} \right)^{1/3} \left(\frac{16}{16} \right)^{0.25} = 1.968 \quad (4.5)$$

and

$$CF_{chord} = \left(\frac{10^{13.358}}{10^{12.476}} \right)^{1/3} \left(\frac{25.4}{16} \right)^{0.25} = 2.209, \quad (4.6)$$

respectively. Values for the low cycle fatigue range ($m_1 = 3.0$) were taken but the factors were found to be the same for the high cycle fatigue range ($m_2 = 5.0$). Finally, the stresses were converted to SCFs according to Equation 1.6, by dividing the maximum stress (σ_{max}) by the nominal stress (σ_{nom}) in the brace for load cases F_x , F_y and F_z . Load case F_z results in pure shear stress in the brace and the SCF is therefore calculated by dividing the maximum stress by the nominal nominal shear stress (τ_{nom}). The nominal normal and shear stresses in the brace were calculated analytically:

$$\begin{aligned} \sigma_{nom, F_x, crown} &= \frac{M_{bending, crown} \cdot x}{I_{xx}} = \frac{10^4 \text{ N} \cdot 1,247 \text{ mm} \cdot 162 \text{ mm}}{1.502 \cdot 10^8 \text{ mm}^4} = 13.5 \text{ MPa}, \\ \sigma_{nom, F_y, saddle} &= \frac{M_{bending, saddle} \cdot y}{I_{yy}} = \frac{10^4 \text{ N} \cdot 1,324 \text{ mm} \cdot 162 \text{ mm}}{1.502 \cdot 10^8 \text{ mm}^4} = 14.3 \text{ MPa}, \\ \sigma_{nom, F_z} &= \frac{F_z}{A} = \frac{10^4 \text{ N}}{12,420 \text{ mm}^2} = 0.805 \text{ MPa}, \\ \tau_{nom, M_z} &= \frac{M_{torsion} \cdot r}{J} = \frac{10^7 \text{ Nmm} \cdot 162 \text{ mm}}{3.004 \cdot 10^8 \text{ mm}^4} = 5.39 \text{ MPa}. \end{aligned} \quad (4.7)$$

4.3 Results and Discussions

In this section, the results are presented and discussed in two parts, corresponding to the methodology. The results of the FE computations simulating the fatigue experiment and the computed equivalent SCFs are discussed in 4.3.1 and 4.3.2, respectively.

4.3.1 Comparison With the Fatigue Experiment

To compare the HSS and ENS approach in terms of accuracy, the number of cycles to fatigue failure was computed using different FE models of a T-joint and the results are depicted in Figure 4.6, where the thick and thin bars represent failure at the chord and brace side respectively. Those results and the corresponding effective stress ranges are listed in Table 4.3. Note that the actual number of cycles to failure for the fatigue experiment cannot be disclosed in this section due to confidentiality reasons, but is discussed in Appendix F. However, there is still much to discuss regarding the comparison between the HSS and ENS approaches based on the FE calculations.

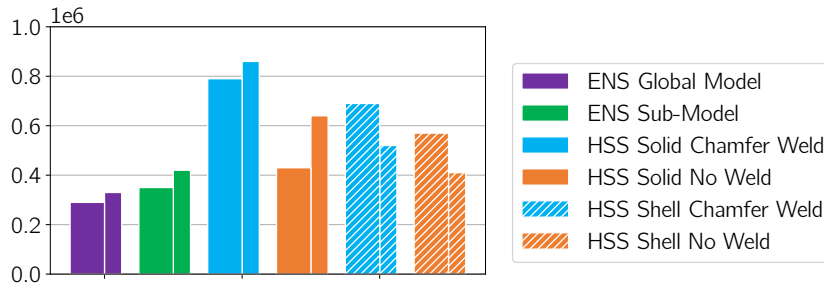


Figure 4.6: Computed number of cycles for failure of the fatigue experiment. The thick and thin bars represent failure at the chord and brace side respectively.

Table 4.3: Computed effective stress ranges and numbers of cycles for failure of the fatigue experiment.

Model name	Element type	Weld profile	$\Delta\sigma_{eff}$ [MPa]		N_{mean} [#]	
			Chord	Brace	Chord	Brace
ENS Global Model	3D		600	577	290,000	330,000
ENS Sub-Model	3D		564	530	350,000	420,000
HSS Solid Chamfer Weld	3D		199	216	790,000	830,000
HSS Solid No Weld	3D		243	239	430,000	640,000
HSS Shell Chamfer Weld	2D		208	256	690,000	520,000
HSS Shell No Weld	2D		221	278	570,000	410,000

It can be observed that the ENS approach provides a significantly lower estimation of fatigue life for the experiment compared to the HSS approach. Notably, the difference is more prominent when analyzing the results of the 'ENS Global Model' and the 'HSS Solid Chamfer Weld' which share a similar FE model geometry in both approaches. This discrepancy can be explained by the S-N curves used in both approaches. Specifically, the HSS T curve is tailored for tubular joints, in contrast to the ENS FAT225 S-N curve. Although the FAT225 S-N curve has demonstrated to fit for different welded straight-plated geometries under the ENS approach, it might not be able to capture the difference between welded straight plates and welded rounded plates, as in a tubular joint. In the case of the latter, the stress is concentrated more along the direction of the weld, potentially leading to an early crack propagation phase and fully penetrated cracks in a relatively later stage. As the FAT225 curve might not be able to account for this variation in stress concentration, the difference in the estimated number of cycles for the 'ENS Global Model' and the 'HSS Solid Chamfer Weld' can be explained.

When comparing the 'ENS Global Model' with the sub-modeling approach, a difference similar to that found in the previous chapter can be observed in the effective stress range, which is approximately 6% lower in the sub-modeling approach. It should be noted that this relative error leads to an overestimation of fatigue life by approximately 20% in terms of the number of cycles required for failure. This is due to the exponential relationship between the stress range and the number of cycles, meaning that even small changes in the stress range can significantly impact the predicted fatigue life.

When comparing the results of the FE models for the HSS approach, higher stresses can be observed when a weld profile is excluded and when 2D elements are used. The exclusion of a weld is expected to cause higher stresses for three reasons. Firstly, the angle at the stress concentration is smaller, resulting in a higher stress singularity effect and subsequently higher stresses. Secondly, more material is presented to divide the concentrated stress over. Lastly, stresses are read further away from the chord or plate, as the weld leg length is not subtracted from the distance between the intersecting plate and the extrapolation points. As the geometry of the intersecting plates causes a stress concentration that becomes lower when looking further away from the intersection, the extra distance to the extrapolation points will result in a lower stress. Optionally, the extrapolation points for the models without weld could be located at the same position along the brace and chord as for the models including the weld. However, no guidelines were found to recommend this and it has therefore been considered out of the scope of this research.

The observed higher stresses for the models composed of 2D elements with respect to 3D elements can be explained by the fact that there is only one layer of nodes present over the thickness for the 2D elements. 3D elements provide more degrees of freedom, allowing for more geometrical flexibility, resulting in less stiffness and lower stresses. As a result, when using 2D elements, the model tends to overestimate the stresses due to the increased stiffness in the thickness direction.

Furthermore, it is remarkable that the models composed of 3D elements predict failure at the chord side, while those composed of 2D elements predict failure at the brace side. The fatigue experiments conducted to derive the T curve demonstrated failure exclusively at the chord side [22]. Considering that in those fatigue experiments, the brace and chord thicknesses and the ratio between them are closely related to the considered T-joint, failure predicted at the chord side is more realistic. This discrepancy between 3D and 2D elements could be attributed to the difference in the connection between the chord and brace. In the models composed of 2D elements, there is only one edge connecting the brace and the chord, resulting in an overestimation of stiffness between them. Additionally, there is no smooth transition of stresses between the brace and the chord. On the other hand, the models composed of 3D elements have at least three nodes along the thickness direction, providing more geometrical flexibility and a smoother transition of stresses. Generally a smaller thickness results in higher stresses, these higher stresses in the brace are compensated for by the connection with the chord for the solid elements but the shell elements do not provide the same level of compensation.

4.3.2 Comparison of the Equivalent SCFs

To compare the ENS and HSS approach from a design perspective, equivalent SCFs were computed for the T-joint and the results are presented in Figure 4.7. The SCFs were determined for the locations where the maximum stress occurs for each load case and the computed SCFs are depicted by thin and thick bars for the brace and chord, respectively.

A similar tendency can be observed for the load cases F_x , F_y and F_z , and the results show to be consistent with those obtained from the comparison with the fatigue experiment in the following aspects three aspects. Firstly, the SCFs computed using the ENS approach are equal to or greater than those calculated using the HSS approach, indicating that there is no increase of the computed fatigue life by using the ENS approach instead of the HSS approach. Additionally, for the HSS approach higher stresses are observed when a weld profile is excluded and when 2D elements are used. Lastly, failure at the chord side is expected when 2D elements are used and failure at the brace side is expected when 3D elements are used, except when M_z is applied. The explanations for these results remain the same as those provided for the fatigue experiment, as discussed in subsection 4.3.1.

Load case M_z shows a different tendency compared to the other load cases. The equivalent SCFs are almost twice as high for the brace as for the chord. This difference originates from the type of loading, which is a torsion moment around the brace axis that generates pure shear in the radial direction of the brace cross-section. The magnitude of the shear stress depends on the polar moment of inertia, which comprises the brace radius and the brace thickness and is constant throughout the length of the brace. At

the location of the connection with the chord, the polar moment of inertia suddenly becomes much larger due to the increased cross-sectional area, resulting in the observed decrease in shear stress.



Figure 4.7: Equivalent SCFs for the T-joint. The thick and thin bars represent the SCF at the chord and brace side respectively.

4.4 Conclusions

The HSS and ENS approaches were compared in terms of accuracy and equivalent SCFs and based on the results obtained, the following conclusions can be made:

- The ENS approach does not lead to an increase in computed fatigue life over the HSS approach for tubular joints. This can be explained by the fact that the FAT225 curve used in the ENS approach is not tailored for tubular joints, in contrast to the T curve for the HSS approach.
- For the HSS approach, the choice of element type and the inclusion of a weld profile have a significant effect on the stress distribution and resulting fatigue life prediction. Using 3D elements with a weld profile included is recommended to obtain the longest computed fatigue lifetime. This can be explained by the increased stiffness in the thickness direction for the 2D elements, and by the higher effect of singularity and the reduction of material to distribute stresses by excluding a weld profile.
- Failure at the chord side is expected when 3D elements are used, while the use of 2D elements results in expected failure at the brace side. Based on the consistent occurrence of fatigue failure at the chord side in comparable tubular joint experiments [22], the use of 3D elements provides a more accurate prediction of the failure location.

5 Conclusions and Further Research

In the final chapter of this thesis, key conclusions and recommendations for further research are presented for the application of the ENS approach on tubular joints.

5.1 Conclusions

The FE mesh configurations for the ENS approach were investigated and the application to a tubular T-joint was evaluated. Specifically, sub-modeling of the ENS approach was investigated and a comparison with the HSS approach in terms of fatigue life was made. Based on this research the following main conclusions can be made:

- For the FE mesh configurations of the ENS approach, it has been found that with a maximum element size in the notch equal to 0.39 mm, according to DNV [1], unacceptable SCF errors are obtained of -4% to 4%. Furthermore, with a maximum notch element size of 0.25 mm, according to IIW [2], SCF errors of -0.3% and -2.2% were obtained, indicating that accurate results can be achieved but are not guaranteed. Additionally, the accuracy of the mesh was found to be primarily influenced by the number of nodes surrounding the notch, rather than the size of the elements in the notch.
- When sub-modeling is applied for the ENS approach on a tubular joint, a global model composed of 3D elements with a weld profile that corresponds to the sub-model should be used. Simplifying the global model by excluding the weld profile or using 2D elements has been found to provide inconsistent and inaccurate results. This is explained by the inaccuracies in the coupled displacement field, originating from the simplifications in the global model. Moreover, a sub-model of the weld area with a size as small as 1.67° of the brace radial angle has been found to provide consistent results still. Thereby, sub-modeling significantly reduces computational costs, compared to the global modeling approach. This is expressed as a reduction in the required mesh size by a factor of 15. Additionally, a rather surprising maximum principal stress error of approximately -6% was observed as a result of sub-modeling for all varied load types and sub-model sizes. The error was found to primarily originate from the sub-model boundaries that intersect the effective notch. Unfortunately, a profound explanation for the magnitude of the error was not found within the author's current knowledge.
- The ENS approach has been found to provide a lower computed fatigue life for tubular joints compared to the HSS approach. This discrepancy can be attributed to the fact that the FAT225 S-N curve used in the ENS approach is derived from fatigue tests of welded straight plates. Therefore, the stress concentration originating from the curved weld profile in a tubular joint is not taken into account. On the contrary, the T curve used in the HSS approach is specifically tailored for tubular joints, originating from tubular joint fatigue experiments. For the HSS approach, various FE models were evaluated, considering the use of 2D or 3D elements and the inclusion or exclusion of a weld profile. Among these models, it was found that a configuration consisting of 3D elements with the inclusion of a weld profile yields the longest computed fatigue life for a tubular joint. This can be explained by the overestimated stiffness in the thickness direction for the 2D elements, and by the higher effect of singularity and the reduction of material to distribute stresses by excluding a weld profile. Finally, conclusions on the accuracy of the computed fatigue lives are disclosed in Appendix F.

5.2 Further Research

Based on the conducted research, the following recommendations for further research were identified:

- **Optimise the ENS mesh.**

The considered optimal mesh configuration for the ENS approach with a notch element size of 0.20 mm and a mesh size of 443,000 nodes for the considered cruciform joint specimen, has shown to be accurate and relatively efficient. However, there are still opportunities for further optimisation

of the required mesh size while maintaining the same level of accuracy. Specifically, the ratio of gradual increase of element sizes could be further investigated to achieve higher efficiency without compromising accuracy.

- **Investigate the sub-modeling error.**

A remarkable sub-modeling error for the ENS approach of -6% was found in this study and gives reason for further investigation. Additionally, a supplementary study was conducted and presented in Appendix D, showing that the -6% error originates from the boundaries intersecting the effective notch radius. This intersection introduced two key factors that possibly cause the error: the presence of small element sizes, leading to numerous elements at the boundary, and the presence of high stress gradients due to the effective notch radius. To gain a deeper understanding of the error's origin, it is recommended to investigate both factors independently. To achieve this, a study can be conducted by creating a global model and a sub-model, both incorporating an effective notch, and ensuring that the highest stresses develop within the notch. In this study, it is recommended to have only one boundary intersecting the effective notch radius. By varying the element sizes and the effective notch radius independently, both effects on the error of sub-modeling can be investigated.

- **Develop an ENS S-N curve for tubular joints.**

The ENS approach generally provides less conservative results compared to the HSS approach, as it captures the stress concentration resulting from the weld profile. However, in the case of tubular joints, the ENS approach was found to yield conservative results compared to the HSS approach. This can be attributed to the derivation of the FAT225 S-N curve used in the ENS approach, which is based on fatigue tests conducted on straight-plated elements. To enhance the accuracy of the ENS approach for tubular joints, it is recommended to develop an S-N curve specifically tailored for this joint type. There are two possible approaches to obtain the ENS S-N curve for tubular joints:

1. The existing fatigue tests conducted to derive the T curve could be utilised. In this case, new FE models are created, incorporating the geometry and details of the tested tubular joints and applying the ENS approach. By comparing the computed stresses with the experimental results, the ENS S-N curve can be composed.
2. New fatigue tests specifically tailored for deriving the ENS S-N curve could be conducted. Previous studies have shown that a minimum thickness of 10 mm is sufficient to accurately capture the notch stresses with an effective notch radius of $r_{ref} = 1$ mm [2]. As thicknesses of T curve fatigue tests vary from 16 mm to 90 mm [22], smaller specimens and corresponding smaller FE models that require less computational costs would be suitable for developing the ENS S-N curve. Additionally, it would be recommended to accurately measure the weld profile of the specimens and match the FE models accordingly.

Bibliography

- [1] DNV-RP-C203 - *Fatigue design of offshore steel structures*. Recommended Practice. DNV, 2019.
- [2] Wolfgang Fricke. "IIW recommendations for the fatigue assessment by notch stress analysis for welded structures". In: *IIW-document XIII-2240r2-08* (2010).
- [3] Electrek. *World's largest offshore wind turbines chosen for first commercial project*. 2021.
- [4] Ørsted. *1991-2001 The First Offshore Wind Farms (Chapter 2/6)*. 1997.
- [5] International Energy Agency. *Offshore Wind Outlook 2019: World Energy Outlook Special Report*. Tech. rep. 2019.
- [6] Walter Musial et al. *Offshore Wind Market Report: 2021 Edition*. Tech. rep. 2021.
- [7] Abdulhakim Adeoye Shittu, Athanasios Kolios, and Ali Mehmanparast. "A systematic review of structural reliability methods for deformation and fatigue analysis of offshore jacket structures". In: *Metals* 11.1 (2020), pp. 1–37.
- [8] Marine Offshore Consultants. *Marine Warranty Survey, Borkum Riffgrund 2 OWF – Suction Bucket Jacket Foundations*. 2017.
- [9] K. Hectors and W. De Waele. "Influence of weld geometry on stress concentration factor distributions in tubular joints". In: *Journal of Constructional Steel Research* 176 (2021).
- [10] Pedersen M. *Introduction to Metal Fatigue*. Tech. rep. 2018.
- [11] C. M. Sonsino et al. "Notch stress concepts for the fatigue assessment of welded joints - Background and applications". In: *International Journal of Fatigue* 34.1 (2012), pp. 2–16.
- [12] M Efthymiou. "Development of SCF formulae and generalised influence functions for use in fatigue analysis, 2nd revision". In: *Offshore Tubular Joints Conference (OTJ'88), USG Offshore Research, Englefield Green Near Egham, United Kingdom*. 1988.
- [13] *ISO 19902 - Petroleum and natural gas industries - Fixed steel offshore structures*. Standard. International Organization for Standardization, 2020.
- [14] DNV-RP-C210 - *Probabilistic methods for planning of inspection for fatigue cracks in offshore structures*. Recommended Practice. DNV, 2019.
- [15] Mostafa Atteya et al. "Experimental and numerical study of the elastic scf of tubular joints". In: *Materials* 14.15 (2021).
- [16] Dieter Radaj, Cetin Morris Sonsino, and Wolfgang Fricke. *Fatigue assessment of welded joints by local approaches*. Woodhead publishing, 2006.
- [17] H Neuber. "Allowance for stress concentration in strength calculations (Structural strength calculations, considering micro and macro stress distributions)". In: *Konstruktion* 20.7 (1968), pp. 245–251.
- [18] Kashif Kamran Toor and Inge Lotsberg. "Assessment of Fatigue Strength of Welded Connections in Thick Plates". In: *International Conference on Offshore Mechanics and Arctic Engineering*. American Society of Mechanical Engineers, 2017.
- [19] J. Baumgartner and T. Bruder. "An efficient meshing approach for the calculation of notch stresses". In: *Welding in the World* 57.1 (2012), pp. 137–145.
- [20] Erkki Niemi, Wolfgang Fricke, and Stephen J Maddox. "Structural hot-spot stress approach to fatigue analysis of welded components". In: *IIW doc* 13 (2018), pp. 1800–1819.
- [21] OTH 92 390. *Background to New Fatigue Guidance for Steel Joints and Connections in Offshore Structures*. 1999.
- [22] Health and London (GB) Safety Executive. *Stress concentration factors for simple tubular joints : Assessment of existing and development of new parametric formulae*. HSE Books, 1997.

A HSS Extrapolation Points

According to DNV-RP-C203 [1], the hot spot stresses for tubular joints should be obtained by linear extrapolation of the stresses assessed at distances a and b from the weld toe, as indicated in Figure A.1 and equations A.1-A.3. Values are given for the considered T-joint, presented in Figure 4.1.

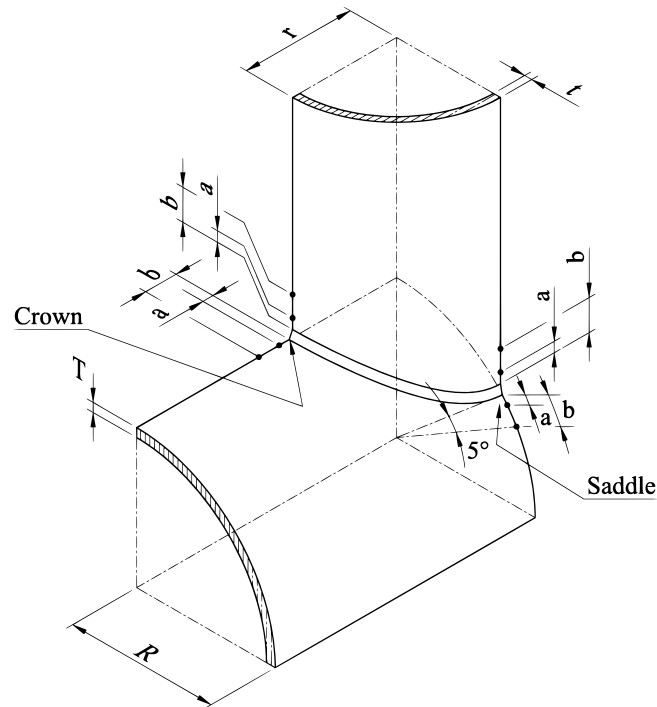


Figure A.1: Points for readout of stresses for the derivation of hot spot stress in tubular joints [1].

For extrapolation of stress along the brace surface normal to the weld toe:

$$\begin{aligned} a &= 0.2\sqrt{rt} = 9.07 \text{ mm}, \\ b &= 0.65\sqrt{rt} = 29.5 \text{ mm}. \end{aligned} \tag{A.1}$$

For extrapolation of stress along the chord surface normal to the weld toe at the crown position:

$$\begin{aligned} a &= 0.2\sqrt{rt} = 9.07 \text{ mm}, \\ b &= 0.4\sqrt{rtRT} = 25.3 \text{ mm}. \end{aligned} \tag{A.2}$$

For extrapolation of stress along the chord surface normal to the weld toe at the saddle position:

$$\begin{aligned} a &= 0.2\sqrt{rt} = 9.07 \text{ mm}, \\ b &= 2\pi R \frac{5}{360} = \frac{\pi R}{36} = 26.6 \text{ mm}. \end{aligned} \tag{A.3}$$

B Variation of the Effective Notch Radius

The effective notch radius was varied for the cruciform joint with dimensions shown in Figure 2.1. The 'rainbow' mesh, shown in Figure 2.2, was applied with a small element size in the notch of 0.07 mm, to minimise meshing errors. The results are presented in Figure B.1 as a difference in SCF, compared to an effective notch radius of $r_{\text{ref}} = 1$ mm.

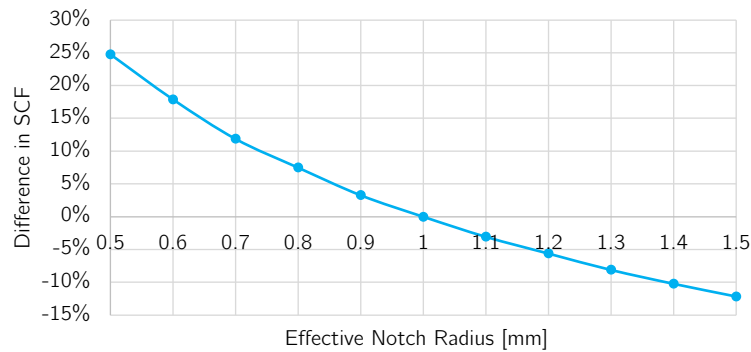


Figure B.1: Variation of the effective notch radius.

A negatively correlated nonlinear relation between the SCF and the effective notch radius can be observed, which corresponds to literature and experimental data [10]. The observed relation can be explained from a computational perspective by the increase of the singularity effect for smaller radii.

Figure B.1 also shows that the SCF is sensitive to variations of the effective notch radius. It is therefore important to note that for the ENS approach with an effective notch radius of $r_{\text{ref}} = 1$, the stresses are fitted to the S-N curve, as explained in subsection 1.5.3. Thus, the stresses obtained from the ENS approach are difficult to interpret without the S-N curve or experimental data, as the stresses are localised to fine detail.

C Displacements Around the T-joint Weld

The results of sub-modeling are influenced by the boundary conditions, which originate from the displacements obtained from the global model. Therefore, the displacements of the global models listed in Table 3.1 have been evaluated to determine appropriate sub-model dimensions perpendicular to the weld, as shown in Figure 3.2a. The maximum displacements at various cross-sections, at distances from the chord and brace, were compared to the maximum displacements obtained from the 'ENS Global Model'. The results are presented as the error in maximum displacement relative to the 'ENS Global Model'.

Based on the results shown in Figure C.1, Figure C.2 and Figure C.3, sub-model lengths of 45 mm, 45 mm and 15 mm have been selected, respectively. In general, the errors in the displacements show a consistent trend over the distances from the chord and brace, suggesting that the dimensions perpendicular to the weld have a minor influence on the accuracy of the sub-modeling.

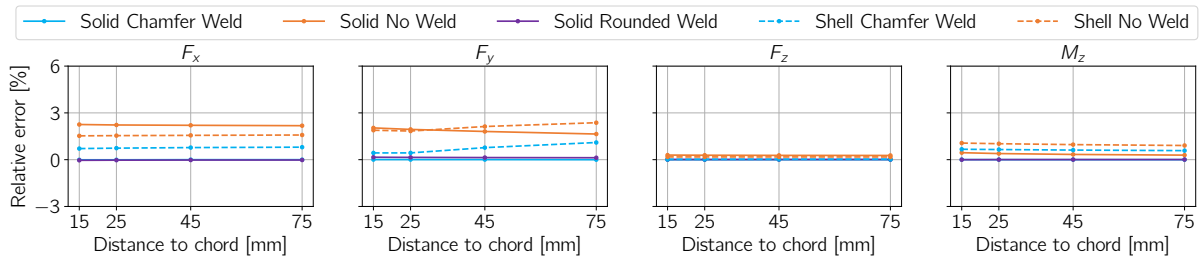


Figure C.1: Error of the maximum displacement at the brace of the global models relative to the 'ENS Global Model' at distances from the chord.

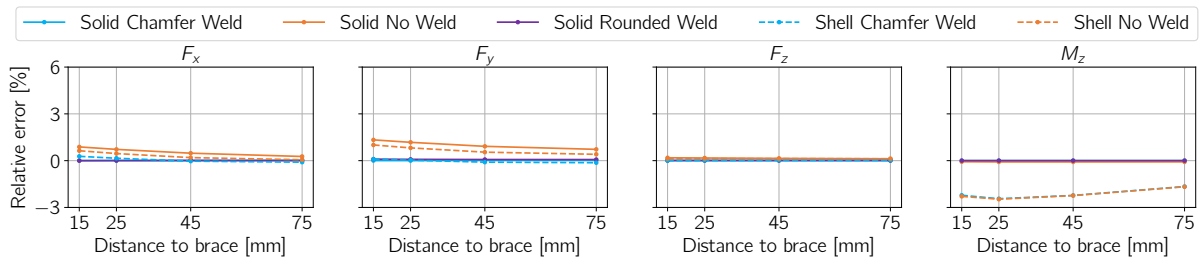


Figure C.2: Error of the maximum displacement of the global models relative to the 'ENS Global Model' at distances to the outside from the brace.

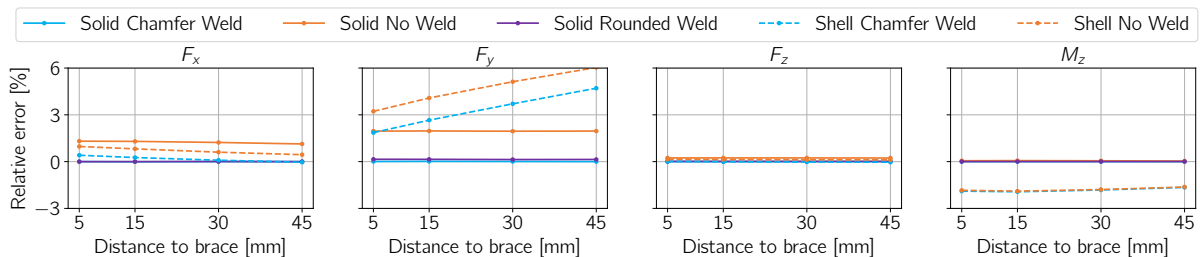


Figure C.3: Error of the maximum displacement of the global models relative to the 'ENS Global Model' at distances to the inside from the brace.

D Supplementary Sub-Modeling Study

This appendix provides the methodology and a brief discussion of the results of a supplementary sub-modeling study conducted to further investigate the -6% error found, as discussed in section 3.3. Furthermore, the study was conducted to validate the sub-modeling approach used.

In this supplementary study, a global model was created consisting of two plates with thicknesses equal to those of the brace and chord of the T-joint. A chamfer weld profile was modeled at the intersection of both plates using the ENS approach and a sub-model was made of the welded area with the same geometry and mesh as the global model. The boundaries are located parallel to the weld and are placed such that no intersection with the effective notch was made. The thicker plate is fixed at the plate end, and a force of 10 kN is applied at the thinner plate end, as shown in Figure D.1.

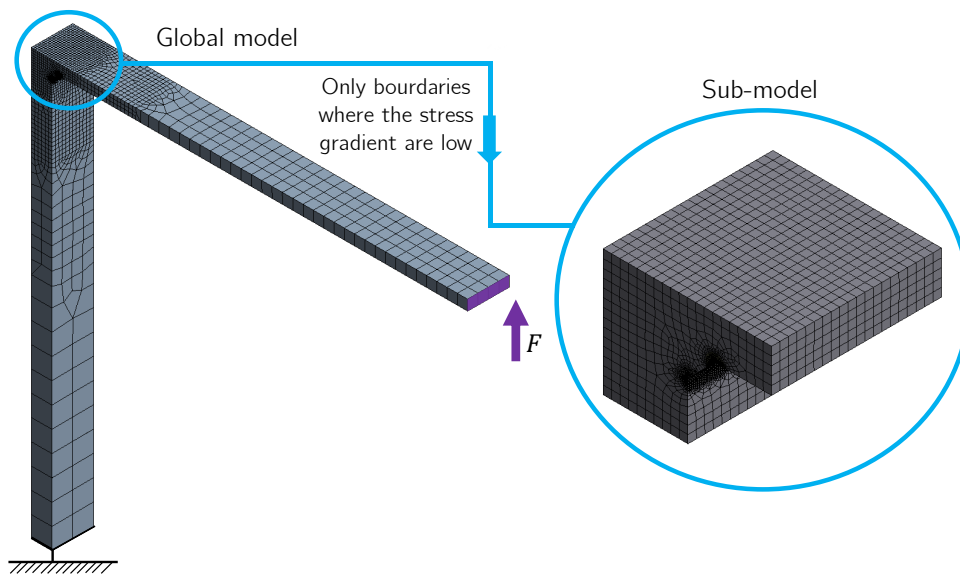


Figure D.1: Setup of the supplementary sub-modeling study.

The stresses and displacements of both the global model and sub-model are compared along the path shown in Figure D.2 and the results are presented in Figure D.3. It can be observed that the sub-modeling errors for the principal stress are only present at the effective notch radii, where the stresses peak. Near the boundaries, the errors in principal stress become negligible. Moreover, negligible errors are observed in the displacements along the entire path.

Therefore, the following two conclusions can be drawn. Firstly, the consistent stress errors of -6% observed across the surface of the T-joint sub-model can be attributed to the boundaries that intersect the effective notch. Secondly, the effective notch introduces a stress error due to sub-modeling. Possibly, the negligible displacement errors that originate from the displacement coupling at the boundaries, are greatly amplified by the singularity effect in the notch.

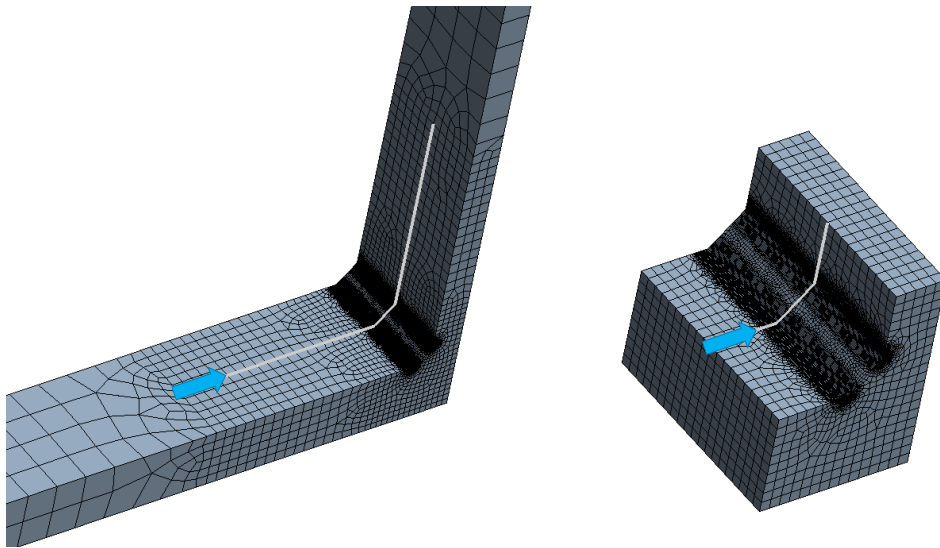


Figure D.2: The evaluated path of the global model (left) and the sub-model (right).

In Figure D.3, the principal stresses and displacements of the global model and the sub-model are plotted for the considered path, and the errors of the sub-model relative to the global model are also shown.

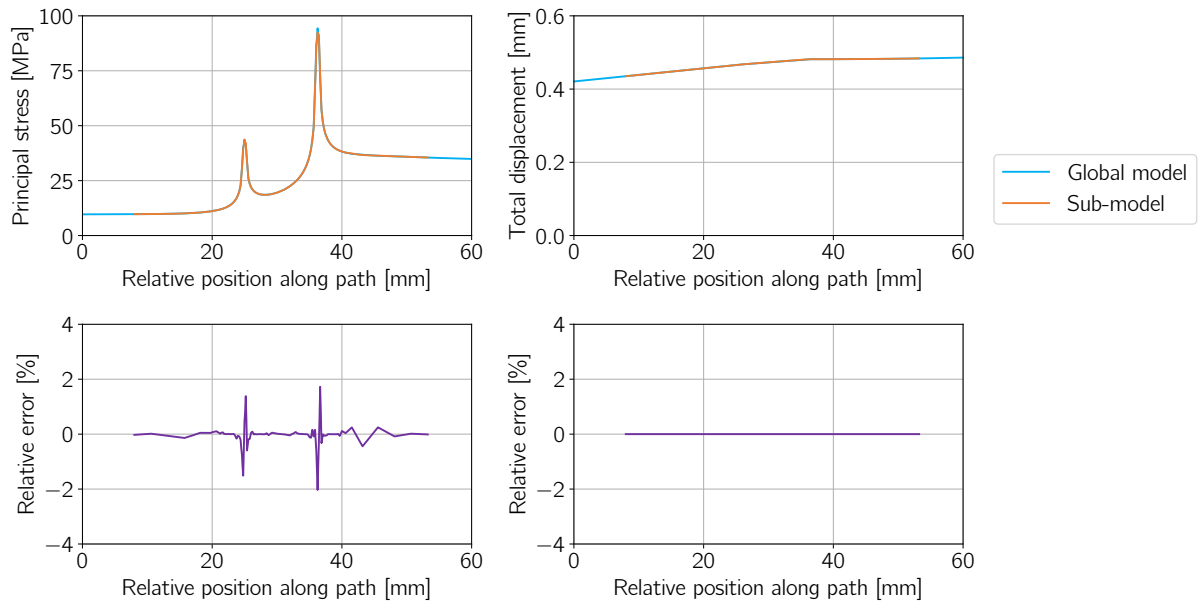


Figure D.3: The maximum principal stresses (upper left), the total displacements (upper right) and the relative errors of the stresses (lower left) and the displacements (lower right) along the path.

E Supplementary Results

This appendix presents and briefly discusses supplementary results of the sub-modeling study and the comparison with the fatigue experiment.

E.1 Sub-Modeling Study

To investigate the impact of larger element sizes in the global model on the accuracy of sub-modeling, the displacements from the 'HSS Solid Chamfer Weld' model were applied to the boundaries of the sub-model. A comparison is made with the 'Solid Chamfer Weld' model, in which only the mesh is different, and with the 'ENS Global Model'. Details of the mesh configurations of the models can be found in Table 3.1 and Table 4.1, and the results are shown in Figure E.1.

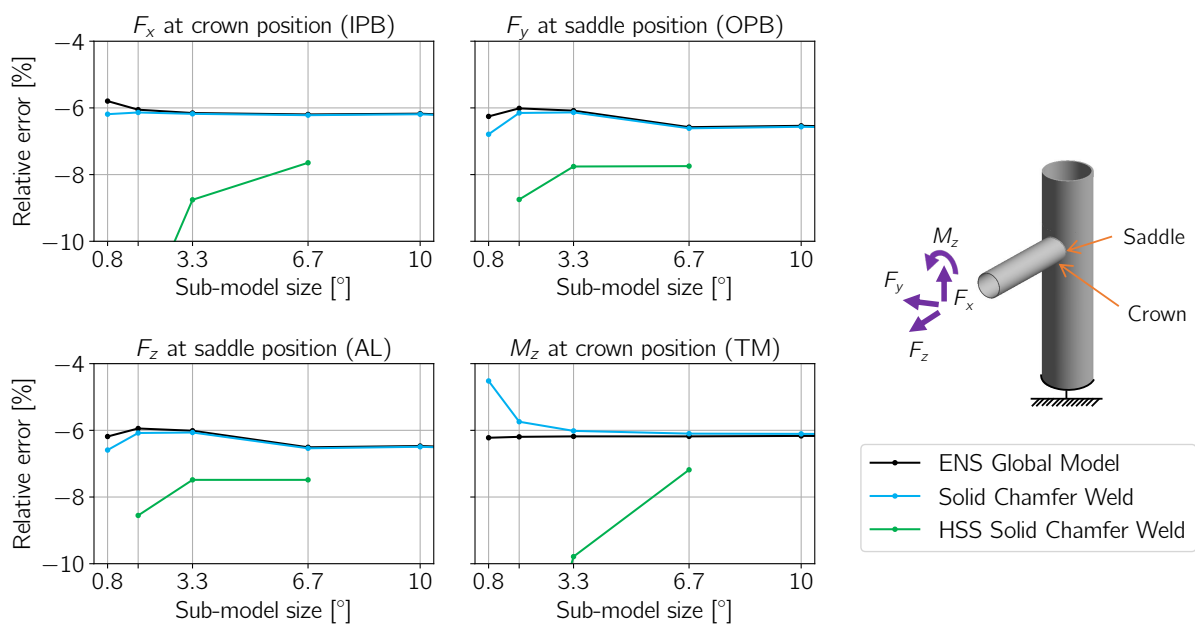


Figure E.1: The relative sub-modeling error due to varying global model element sizes.

Larger sub-modeling errors can be observed with the sub-model boundaries coupled to the 'HSS Solid Chamfer Weld' model, indicating that the used element sizes for the global model are too coarse. However, for a sub-model size of 6.7° consistency can be observed with an error close to -8%, suggesting that the combination of sub-model size and global model mesh can be utilised when the error is taken into account. The difference in element sizes between the 'Solid Chamfer Weld' and 'HSS Solid Chamfer Weld' models provides room for further optimisation of the element sizes of the global model but is considered out of the scope of this thesis.

To investigate the consistency of the sub-modeling error of -6% at the locations along the weld where stresses are lower, the relative errors due to sub-modeling for both the crown and saddle positions are plotted for all load cases in Figure E.2. The results show that the error remains consistent except for the in-plane bending (IPB) load case at saddle position, where an error of approximately -5% is observed. However, this discrepancy is still closely related to the overall trend.

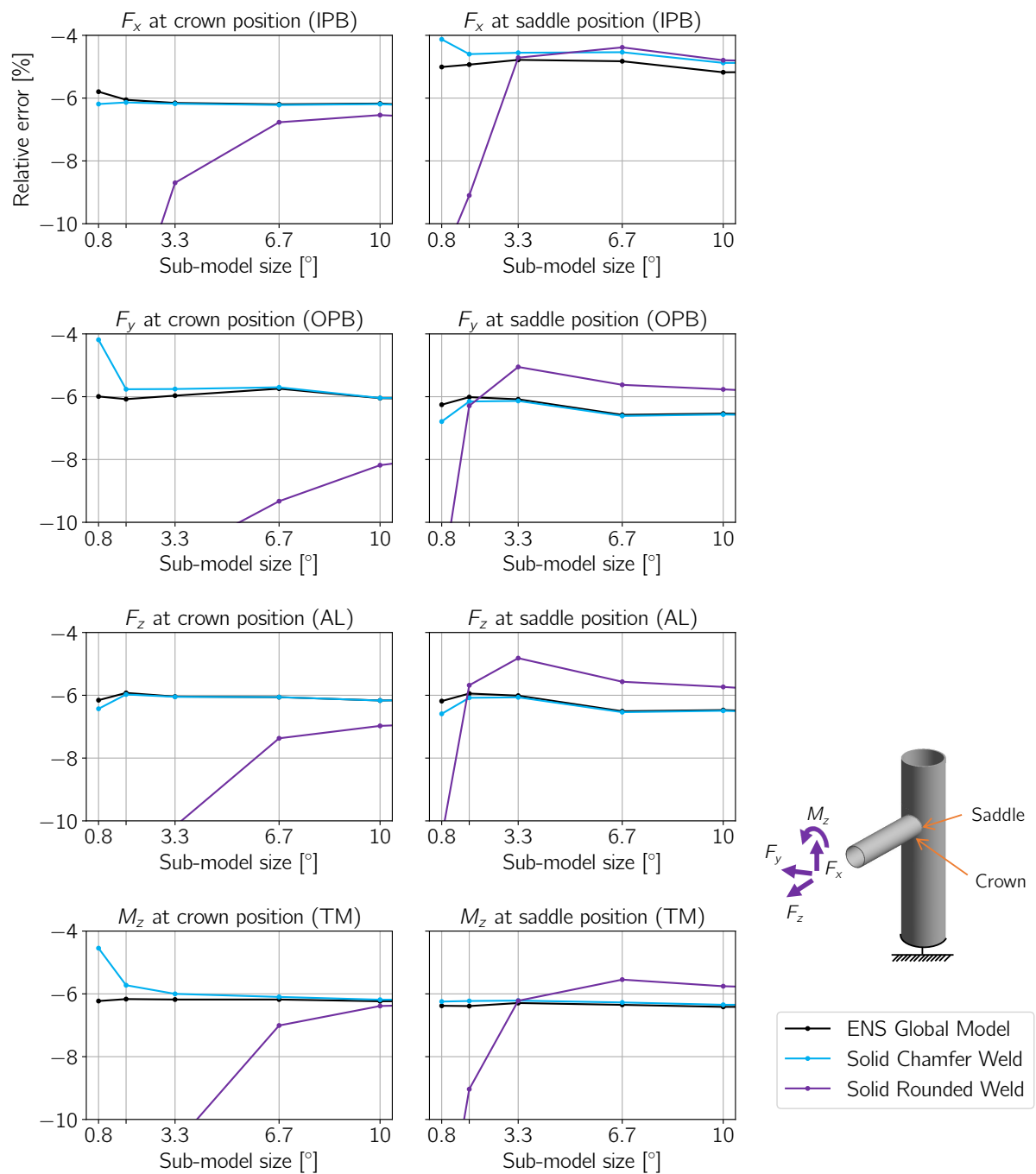


Figure E.2: The relative sub-modeling errors at saddle and crown positions for the consistently performing sub-modeling approaches.

To gain a deeper understanding of the -6% error originating from sub-modeling, the stresses and displacement of several elements were evaluated for the 'ENS Global Model' and the sub-model with displacements coupled to that same model. Figure E.3 shows one of the evaluated elements. A similar correlation was found for the elements, where the displacement errors are close to 0% and the stresses show errors of approximately -6%.

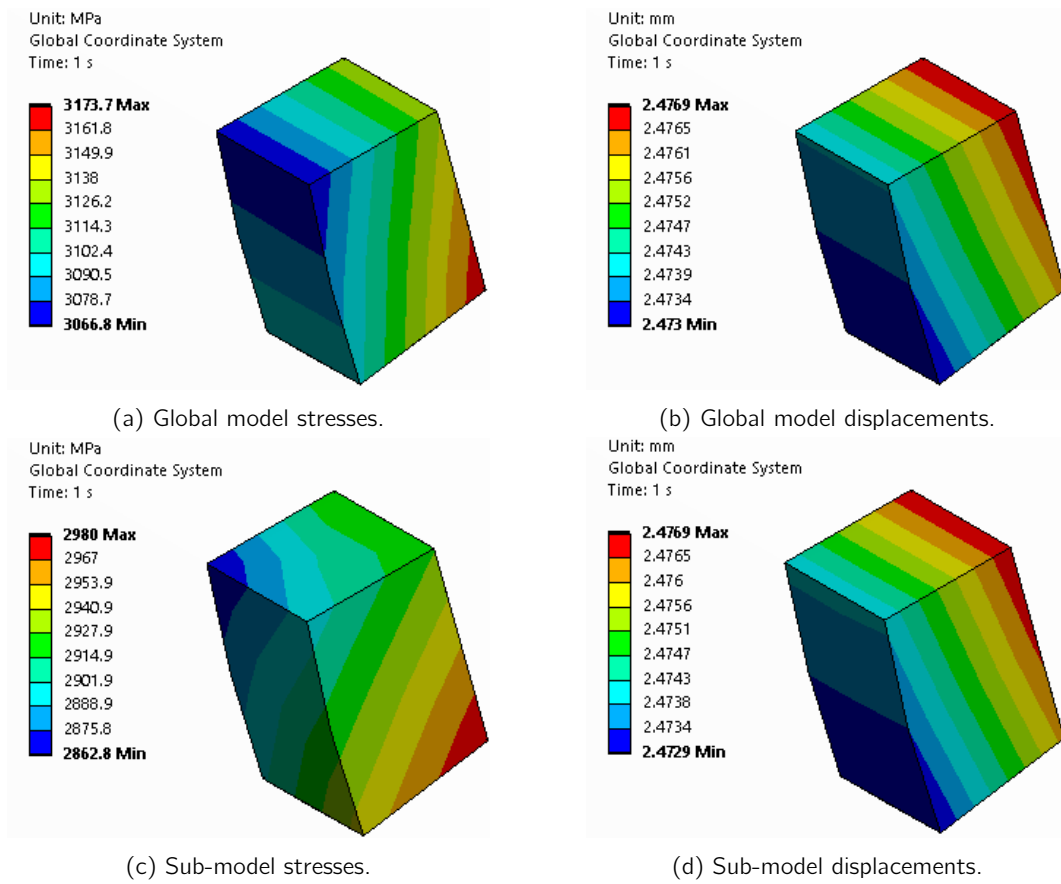


Figure E.3: Normal stresses and displacements in x-direction for an element located at the surface along path 1 at a distance of 2.5 mm from the effective notch radius.

E.2 Comparison With the Fatigue Experiment

The extended results of the computations for the comparison with the fatigue experiment are shown in Figure E.4. The effective stresses and the individual contributions of F_x and M_z to the effective stress are plotted. It can be observed that the fatigue results are mainly influenced by the contribution of F_x , which explains why failure is expected to occur at the chord side, while the contribution of M_z predicts failure at the brace side.

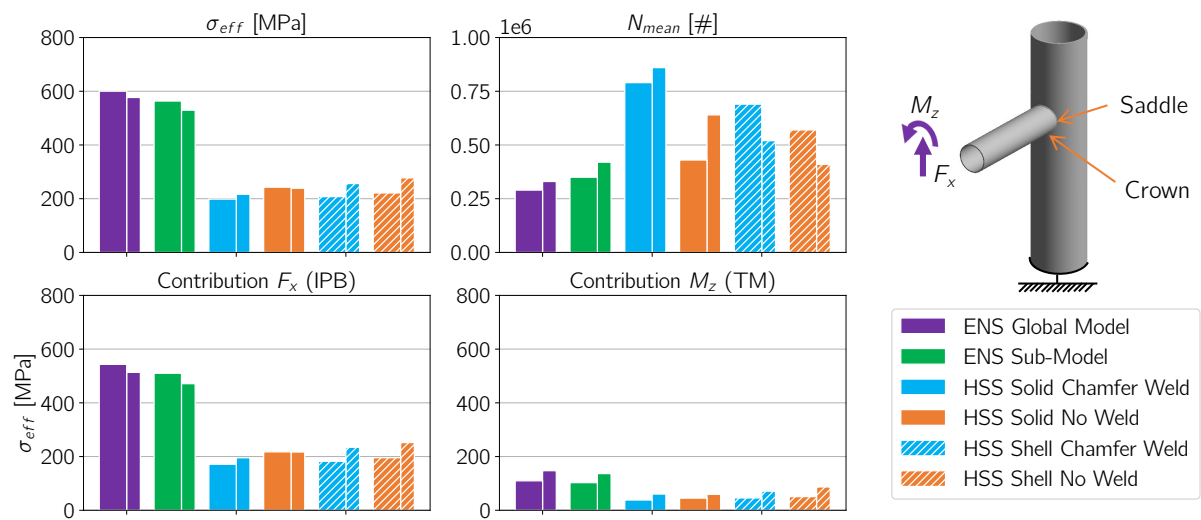


Figure E.4: Supplementary results of the computations for the comparison with the fatigue experiment. The thick and thin bars represent the SCF at the chord and brace side respectively.

F Results T-Joint Experiment (Confidential)

This appendix is not included in this version of the report due to confidentiality restrictions.